Available online at www.sciencedirect.com

Journal of Nuclear Materials 345 (2005) 109–135

www.elsevier.com/locate/jnucmat

Radiation damage effects in candidate titanates for Pu disposition: Pyrochlore

D.M. Strachan *, R.D. Scheele, E.C. Buck, J.P. Icenhower, A.E. Kozelisky, R.L. Sell, R.J. Elovich, W.C. Buchmiller

Pacific Northwest National Laboratory, P.O. Box 999, 902 Battelle Boulevard, Richland, WA 99352, United States

Received 8 February 2005; accepted 8 April 2005

Abstract

Laboratory experiments on titanate ceramics were performed to verify whether certain assumptions are valid regarding the swelling, chemical durability, and microcracking that might occur as ^{239}Pu decays. Titanate ceramics are the material of choice for the immobilization of surplus weapons-grade Pu. The short-lived isotope ^{238}Pu, was incorporated into the ceramic formulation to accelerate the effects of radiation-induced damage. We report on the effects of this damage on the density (volumetric swelling <6%), crystal structure of pyrochlore-bearing specimens (amorphous after about 2×10^{18} α/g), and dissolution (no change from the fully crystalline specimen). Even though the specimens became amorphous during the tests, there was no evidence for microcracking in the photomicrographs from the scanning electron microscope. Thus, although pyrochlore is susceptible to radiation-induced damage, the material remains chemically and physically viable as a material for immobilizing surplus weapons-grade Pu.

1. Introduction

In the 1990s, discussions were held between representatives of Russia and the United States on the disposition of surplus weapons-grade plutonium [1,2]. In parallel, the US Department of Energy (DOE), after completion of a preliminary environmental impact statement, decided to build three plants at the Savannah River site in west central South Carolina to implement a program to provide for the safe and secure storage of surplus weapons-grade Pu. In the first of these plants, Pu from weapons declared to be excess will be converted to PuO_2 at the Pit Disassembly and Conversion Facility. The PuO_2 will then be converted to a mixed oxide (UO_2 and PuO_2) nuclear fuel at the Mixed Oxide Fuel Fabrication Facility and 'burned' in a commercial nuclear reactor. Some of the Pu declared to be excess was not in weapons, was not in a form that was acceptable at the Pit Disassembly and Conversion Facility or directly acceptable at the Mixed Oxide Fuel Fabrication Facility, and was, therefore, destined for a third facility called the Plutonium Immobilization Plant. In 2002, at the request of the Administration, DOE undertook a review of the options to restructure the US Pu disposition program to address the concerns by the Administration regarding the cost of both the Russian and US programs. As a result of the review, the immobilization option was dropped [3]. In the meantime, the development of a concept for the immobilization of some weapons-grade Pu

---

* Corresponding author. Tel.: +1 509 3760677; fax: +1 509 3763108.

E-mail address: denis.strachan@pnl.gov (D.M. Strachan).

0022-3115/$ - see front matter © 2005 Elsevier B.V. All rights reserved.
doi:10.1016/j.jnucmat.2005.04.064

was ongoing [4–7]. In this program, a titanate ceramic containing approximately 10 mass% Pu was developed [7]. The immobilized Pu ceramic was to be placed in stainless-steel cans that would be sealed and hung on a rack inside a large canister, approximately 0.6 m in diameter and 3 m tall, and the remaining volume filled with high-level nuclear waste glass [2]. This package provided secure interim storage for the Pu because the Pu is difficult to recover from the titanate ceramic, and the high-level waste glass forms a radiation barrier that makes retrieval difficult at any place other than a heavily shielded facility. This 'can-in-canister' would be shipped to the national nuclear waste respository that is currently under development at Yucca Mountain, which is located north of Las Vegas, NV.

Once this canister is placed in the repository, the main concern is with the possibility of a nuclear criticality event [8]. As produced, there are sufficient neutron absorbers (Gd and Hf) in the titanate ceramic that it can be stacked safely in an infinite array and with full moderation from water. However, once these canisters begin to fail some 10000 years after burial, the concern is that the neutron absorbers and fissile, either ^{239}Pu or its decay product ^{235}U, stay together so that criticality cannot occur for the long-term [8]. A preliminary performance assessment suggested that a criticality event was very unlikely given certain assumptions about the behavior of the ceramic [8]. Assumptions had to be made concerning the swelling, chemical durability, and microcracking that might occur as the ^{239}Pu decays, similar to what occurred in PuO_2 and zirconolite [9,10]. The assumptions that were made in this 'safety case' needed to be verified through laboratory experiments and are the purpose of the experiments described here.

Even though the immobilization option was dropped and the development of a Pu-immobilization form was stopped, the possibility existed that a Pu-immobilization form could be needed in the future. Radiation-damage experiments are very long-term and, at the time of the decision to drop the immobilization-form development, radiation-damage experiments had been underway for about 4 years. To stop the radiation-damage experiments at that time would mean that, if there were a future need, the experiments would have been started from the beginning. The completion of the radiation-damage studies was critical in validating the assumptions made in determining the acceptability of the ceramic in the proposed repository environment. If the ceramic in the fully damaged state were not to perform as predicted, the ceramic would probably prove not to be an acceptable form for immobilization. Thus, a decision was made at DOE to continue the radiation-damage experiments so that a package of data was available to support any future decision on the use of a titanate-based immobilization form.

As ^{239}Pu decays with the emission of an alpha particle, the recoiling ^{235}U atom causes extensive damage to the surrounding chemical bonds, destroying about 1000 bonds before coming to rest [11,12]. To study this effect in the laboratory, two techniques are typically used. The first is to place a specimen in an accelerator and bombard it with heavy ions such as gold or xenon. This causes rapid damage in the first 10 s of micrometres of the surface. While the effect on the crystal structure of the ceramic is accomplished, bulk effects, such as swelling and cracking, are not manifest. In the second method, a short-lived isotope such as ^{244}Cm (half life of 18.1 years) and ^{238}Pu (half life of 87.7 years), are incorporated into the ceramic formulation. We selected this second method because we needed information on the changes in bulk properties such as dimensions, densities, and chemical durability. We selected ^{238}Pu because of its obvious chemical similarity to the ^{239}Pu that was to be immobilized.

Several radiation-damage studies have been performed on synthetic pyrochlores. The cubic structure (Fd3m) of pyrochlore ($A_2B_2O_7$) can take on many compositions through charge compensation between the A and B sites [$A(III)_2\ B(IV)_2O_7$ and $A(II)_2B(V)_2O_7$, as examples] or on the A site alone [$A(II)_{0.5}A(IV)_{0.5}$-$B(IV)_2O_7$, as an example]. In the case of Pu immobilization, the B site is occupied by Ti, principally, and the A sites by Gd, Hf, U(IV), Pu(IV), and Ca [7,12]. Studies on ^{244}Cm-substituted pyrochlore have shown that the pyrochlore structure becomes amorphous between 3×10^{18} and 4×10^{18} α decays/g (hereinafter α/g) when Ti occupies the B site [11,13–16] and, from ion-beam irradiation studies, greater than 3×10^{20} α/g when Zr occupies the B site [17]. Pyrochlores with similar composition to that reported here have been reported to become amorphous between 1.5×10^{18} and 2×10^{18} α/g [18–23]. These pyrochlore structures have been observed to swell between 3% and 10% during the process of becoming amorphous from radiation-induced damage [11,14,18–20,24]. Microcracking was not observed [24]. Wald and Offerman [24] found that the bulk dimensions of a 3 mass% ^{244}Cm-bearing $Gd_2\ Ti_2O_7$ swelled 5.5% (revised in Weber and Ewing [23]) when a dose of 3.2×10^{18} α/g was accumulated. The saturation swelling in the Cm-doped $Gd_2Ti_2O_7$ has been determined as a function of porosity and is estimated to approach 6.5% at theoretical density [14]. The unit-cell volume exhibits swelling of 5.1% when a dose of 3.1×10^{18} α/g accumulated [16,25]. A smooth transition between crystalline and amorphous states was observed; no fluorite phase or microcracking were observed [25]. In other work, principally with lighter Kr and Xe ion bombardment, authors report a transition from pyrochlore to disordered fluorite before the test specimen became amorphous [26–30]. Clinard observed severe cracking in $^{238}PuO_2$ [9] and in polycrystalline, ^{238}Pu- bearing zirconolite [10,31] specimens. Aqueous dissolution rates have been observed to increase relative to specimens that are undamaged [14,15,18,19,25,32] and to increase in metamict (amorphous) natural samples [33,34].

Studies on the radiation-damage effects in natural pyrochlores were summarized recently by Lumpkin [35] in an extensive review article covering natural pyrochlore, zircon, zirconolite, brannerite, and perovskite. In this report, Lumpkin [35] reports that natural pyrochlore becomes metamict at 1×10^{16} α/mg (1×10^{19} α/g) and residual diffuse maxima in the X-ray diffraction (XRD) patterns at d-spacings of 0.350–0.363 nm and 0.206–0.222 nm. The latter came from the metal–metal distance and the metal-to-oxygen distance, respectively. The saturation dose was reported to be 1.2×10^{16} α/mg (1.2×10^{19} α/g).

Stability and metastability fields for Ce-, Gd-, Hf-, and U-bearing pyrochlores have recently been determined [36,37]. These thermodynamic property determinations show that the formulation that was to be used in the immobilization of Pu was stable with respect to the constituent elements, constituent oxides, and a mixture of perovskite, metal oxide, and TiO_2. Depending on the composition of the pyrochlore, it might be metastable with respect to perovskite, metal oxide, and TiO_2. Therefore, at a low temperatures similar to those of the repository, some pyrochlores might be unstable thermodynamically with respect to mixture of perovskite, metal oxide, and TiO_2. At the low final temperatures of the repository, however, the kinetics of decomposition is expected to be exceedingly slow, but in the presence of radiation-induced damage and the temperatures during the thermal period, this kinetics could be enhanced.

In this publication, we report on the effects of radiation damage to the density, crystal structure, and dissolution of specimens in which the main phase was pyrochlore. The specimens also contained Hf-rutile [$(Ti_{1-x}Hf_x)O_2$] and some contained zirconolite [ideally, $CaZrTi_2O_7$] and brannerite [ideally, UTi_2O_6]. Some specimens were formulated to have more than trace quantities of zirconolite. While pyrochlore was the phase of choice for the plutonium immobilization ceramic, formulations that gave mixtures of all phases were considered because of the heterogeneity of the Pu feed stock. Overall, in this study, we had 120 ^{238}Pu-bearing specimens each containing about 50 GBq of ^{238}Pu and 80 specimens containing ^{239}Pu. These specimens were stored at three temperatures. The number of specimens and compositions in this study make it much different than other studies reported to date.

2. Experimental methods

Leading up to the preparation of the test specimens, we prepared numerous samples from non-radioactive components, namely Ce, Hf, and Gd. The latter two were also included in the formulations with Pu and U because they are neutron absorbers. In this paper, we briefly describe the methods used to prepare the ^{238}Pu- and ^{239}Pu- bearing ceramic specimens; additional details may be found in Strachan et al. [38]. Reagent-grade constituent oxides and hydroxides, except Pu, were mixed to the correct proportions. The Pu was added as a nitrate solution to the powder. About 100 mL of demineralized water were added, and the mixture was ball milled with zirconia grinding media for 16 h. The resulting wet powder was quantitatively transferred to a beaker with demineralized water and, through various stages of drying, was subsequently dried in an oven at 110 °C. The resulting mixture was pressed into pellets 12.5 mm in diameter. These pellets were then sintered at 1350 °C under flowing Ar gas for 4–8 h, yielding pellets with nominal diameters of 10 mm and heights of 2–3 mm (^{238}Pu-bearing specimens) or 3–4 mm (^{23}Pu-bearing specimens). We prepared the ^{239}Pu-bearing specimens first (15 and 19 May 1999) then characterized randomly selected specimens to make sure that we had our preparation procedures correct. Batches containing ^{238}Pu-bearing specimens were prepared on 25 May 1999, 7 June 1999, 8 October 1999, and 19 October 1999. A number of these specimens were sintered at 1350 °C for an additional 110 h to coarsen the microstructure (16 August 1999 [^{238}Pu] and 6 August 1999 [^{239}Pu]). Ceramics with a coarse microstructure were thought to be more susceptible to microcracking than ones with a fine microstructure. After the specimens were sintered, at least one surface was polished to a 600-grit finish on SiC paper in a small polishing machine. Specimens that were to be tested in the dissolution test had both faces polished. The resulting P1 and PB1 ceramic specimens were not analyzed for composition; the target compositions are shown in Table 1. Molybdenum was added to the formulation to serve as an indication of the behavior of the matrix in the dissolution experiments, in which the pH was greater than 5. Below that pH, the sorption of Mo on anatase, an alteration product for these ceramics at all pH values, becomes significant [39]. The P1 specimens were formulated to contain only pyrochlore and a small amount of Hf-rutile; the PB1 specimens had slightly more TiO_2 and UO_2 than the Pl specimens; this change caused zirconolite and brannerite to form while keeping pyrochlore as the major phase. The '238' and '239' labels refer to the Pu isotope. Two formulations (P1 and PB1) were used to more accurately represent the Pu feed stock at the Plutonium Immobilization Plant.

The PuO_2 concentrations correspond to 10.9 and 10.5 mass% Pu for P1 and PB1 ceramics, respectively. For the P1 specimens, this target composition suggests a formula $Ca_{1.16}Gd_{0.23}\ Hf_{0.30}Pu_{0.24}U_{0.42}Ti_2O_7$. However, some Ti must appear as Hf-rutile, (Hf, Ti)O_2, and some Hf must be on the pyrochlore B site. Thus,

Table 1
The target oxide composition of the pyrochlore ceramics used in this study

Component	P1-238[a]		P1-239		PB1-238		PB1-239	
	mass%	mol%	mass%	mol%	mass%	mol%	mass%	mol%
CaO	12.0	24.8	12.0	24.91	9.91	21.13	9.94	21.15
Gd_2O_3	7.65	2.44	7.64	2.44	7.95	2.62	7.94	2.61
HfO_2	10.8	5.98	10.8	5.98	9.61	5.46	9.63	5.46
MoO_3	0.10	0.09	0.10	0.09	0.11	0.10	0.10	0.10
PuO_2	12.3	5.27	12.3	5.27	11.84	5.24	11.88	5.23
TiO_2	36.1	52.3	36.1	52.38	36.70	54.89	36.82	54.99
UO_2	20.8	8.93	20.8	8.92	23.88	10.57	23.67	10.46

[a] '238' refers to specimens made with ^{238}Pu; '239' with ^{239}Pu.

the approximate actual formula should be $Ca_{1.13}Gd_{0.22}Hf_{0.12}Pu_{0.24}U_{0.40}(Ti_{1.90}Hf_{0.10})O_7$ and 20 mass% TiO_2 with 10% of the Ti replaced with Hf, i.e., $Hf_{0.1}Ti_{0.9}O_2$ [40]. In this formulation, we assumed that Pu(IV) and U(IV) are the relevant oxidation states. Placing the Hf on the B site is consistent with several studies of the Ti- and Zr-bearing pyrochlores [41–44] and references within these publications. Although there are reports about the presence of other oxidation states for Pu and U, notably U(V) and Pu(III) [40,44–46], we did not attempt to design a formula with these oxidation states. We were unable to obtain an accurate analysis of the phases and their respective amounts because we did not have an instrument with which we could analyze these radioactive ceramics. Using this formulation (80 mass% $Ca_{1.13}Gd_{0.22}Hf_{0.24}U_{0.40}(Ti_{1.90}Hf_0)O_7$ and 20 mass% $Hf_{0.1}Ti_{0.9}O_2$) for the pyrochlore specimens, we calculated a theoretical density of 6.008×10^3 kg/m^3 (see Section 3.4 below for the lattice parameter). No such break down of the phase assemblage was possible for the PB1 specimens.

When we started the testing, we predicted that the effects of radiation damage would take a year or two to become manifest. Russian workers, however, saw radiation-damage effects within days of making their specimens [20,47,48]. By the time we obtained our first measurements, a substantial amount of radiation-induced damage had occurred. Therefore, after approximately 2 years of characterization and testing (April 2002), we resintered selected specimens at 1350 °C for 2 h under flowing argon to remove the damage that had occurred and establish the original crystallinity to the specimens. During that time, approximately 1.5% of the ^{238}Pu had decayed to ^{234}U. This small change in the Pu and U contents was ignored during the study of the resintered specimens.

Between characterization and testing that occurred approximately semiannually for the original specimens and up to twice weekly for the resintered specimens, the specimens were housed in stainless-steel vessels in ovens. Each vessel contained either three or four specimens. Three storage temperatures were used ambient (~20 °C),[1] 125 and 250 °C. These temperatures were selected so that some data would be available to estimate the critical temperature – the temperature at which the damage is annealed at the same rate as it occurs. The specimens were stacked so that the specimens had at least one face that would be a near representation of material far from the surface of the specimen. While the alpha particle and the recoiling atom do not travel great distances in the solid, these particles are lost at a free surface, resulting in a gradient in damage production from the free surface inward to the depth of the maximum range of the particles. For alpha particles, this range is 10 s of micrometres, while for the recoiling atom, the range is 10 s of nanometres. Since the damage effects at a free surface do not represent the damage effects in the bulk of the specimen, the specimens were stacked face-to-face so each surface received uniform damage and became more representative of the bulk, similar to procedures originally developed for ^{244}Cm-bearing specimens [13–16].

Because the specimens were highly radioactive, we needed to control the spread of contamination. We also needed to use the same specimen for each XRD measurement. Therefore, we developed an XRD specimen holder for obtaining the diffraction patterns from the polished surface of the specimens. This specimen holder is described in detail elsewhere [49]. This specimen holder and a mounting jig allowed us to locate the specimen in exactly the same position each time it was mounted for examination. The rotational orientation varied each time. To compensate for changes in instrument sensitivity, such as X-ray tube degradation and X-ray tube changes, a disk approximately 25 mm in

---

[1] An oven was used but with no power. The oven served as a cabinet to safely house the specimen storage devices. There was sufficient power generated in three ^{238}Pu-bearing specimens to raise the temperature of the 500 g stainless -steel vessel by about 2 °C.

diameter of the Standard Reference Material 1976 (corundum) from the National Institute of Standards and Testing was permanently affixed to the post of a specimen holder. A reference diffraction pattern was obtained at the beginning and end of each day that patterns were being obtained from the test specimens. The XRD unit was a scintag PAD V (Scintag Corp., Cupertino, CA).

We also developed a laser-based device for measuring the diameter and height of the specimens; it is described elsewhere [50]. Again, because these specimens are highly radioactive, we needed to minimize the time they were handled and the possibility of contamination spread. This device consists of two orthogonal laser curtains and associated detectors (Keyence Corp., Woodcliff Lake, NJ, Model VG 036T and control Model VG 30). With these lasers, we are capable of a resolution of 10 μm. Since we were interested in the relative change in each specimen with time, we were not interested in the absolute accuracy of the instrument, but its long-term stability. To make sure we understood the drift of the instrument, a 'check pellet' was made from stainless steel with a nominal diameter of 10 mm and a nominal height of 2.5 mm. For the period of 664 days, the average diameter of the 'check pellet' was 10.063(6) mm[2] an the height was 2.487(7) mm. This indicated excellent stability. Over the same time, the absolute accuracy was 0.30(7)% and 0.5(3)% for the diameter and height, respectively. We anticipated on the order of 1% swelling in the test specimens. Therefore, the degree of stability and precision of our instrument indicated that we could reliably report 0.1% changes in specimen dimensions.

From the dimension measurements and the mass of the specimen, we can calculate the bulk density. In reality, however, the table on which the specimens sat during the measurements had about a 20 μm wobble up and down. While this wobble slightly degraded the accuracy of the overall height measurement, it, in combination with the chips on the edges of the specimens (see the discussion below), resulted in unacceptable uncertainty in the calculated bulk densities. Therefore, as discussed below, we do not report the changes in bulk density calculated from the observed changes in specimen dimensions. We do report the changes in the diameters of the specimens, which are unaffected by the wobble in the table, and from those changes and the assumption of uniform swelling, we calculate the change in the bulk density.

Densities were also measured with a helium pycnometer (Micromeritics, Norcross, GA, Model AccuPyc 1330) With this device, the volume of a weighed specimen is measured by displacement of He gas. The measurements reported here were obtained with an ultraprecise procedure in which a value for the density is not determined until five successive determinations agree within 0.05%. The results, the so-called 'true' density, are sent to a computer where they are automatically stored in a file. For the ^{238}Pu-bearing specimens, three specimens are used in the density determination and two for the ^{239}Pu-bearing specimens. With approximately 0.3 g of ^{238}Pu in the pycnometer, we were concerned that there would be an effect from the radiodecay heat generation. Results from several runs in which the specimens remained in the pycnometer over long times showed that there was an insignificant change in the measured density. The 'true' density is the specimen density, including any closed porosity, but excluding any open porosity.

At the start of the project, we did not have a scanning electron microscope (SEM) in which we could examine specimens containing high concentrations of ^{238}Pu. By the end of the project, we were able to examine these materials. Examinations were performed on a JEOL840 equipped with a Gatan Digital Imaging System, a Robinson Backscattered Detector, and an Oxford ISIS EDS system. For all specimens containing ^{238}Pu there is a significant X-ray background from the decay product ^{234}U. Therefore, the background spectrum collected with the electron beam off was not considered to be interference in the collected X-ray data at lower energies (<10 keV); however, the background spectra were subtracted from some collected spectra before analysis. All collected spectra were saved as data text files. Quantitative analysis was not possible because of the overlap of the Pu and U M lines. The spectra were plotted with a graphing software program. Many of the EDS spectra were severely masked by X-rays from the decay of ^{238}Pu to ^{234}U. This energetic event generates U X-rays. The higher energy L X-rays were more apparent in the collected spectra as these X-rays are more penetrating than the M X-ray lines. To reduce this problem, the smallest possible ceramic sample was used that could still be observed and polished in a glovebox.

In our initial set of experiments with the ^{238}Pu-bearing specimens, we used a modified single-pass flow-through (SPFT) apparatus in which Teflon® reaction vessels and fluid exchange lines were used. However, even adding a platinum liner to shield the Teflon vessel from the alpha radiation, we found that significant (10–100 mg/l) concentrations of fluoride were present in the effluent solutions that were not present when the specimens contained no Pu or only ^{239}Pu. If we continued with this apparatus, the presence of fluoride in the effluent would always cloud the validity of any conclusions we would make about the dissolution of these ceramic materials. Therefore, for the experiments with ^{238}Pu-bearing materials, we replaced the Teflon-based apparatus with one constructed of titanium. We

---

[2] The number in ( ) represents the $1-\sigma$ standard deviation in the last place of the number reported.

continued to use the Teflon apparatus for non-radioactive specimens and for those containing ^{239}Pu.

Basically, the two designs are operated in the same manner. One is constructed with a 40 mL Teflon vessel in which the specimen is tested with Teflon tubing through which solutions pass. The other is constructed of a custom made, 20 mL titanium vessel and small-bore titanium tubing. A gold compression gasket is used as a seal for the titanium vessel. The Teflon vessels are heated in a convection oven; the titanium vessels in an aluminum heater block. Both are controlled to ±2 °C, but the upper limit on the aluminum heater is 85 °C. Syringe pumps (Kloehn; model 50300) were used to transfer solution from the input reservoir bottles to the reaction vessels. Nitrogen gas was used to purge the free space in the solution reservoir to mitigate the effect of atmospheric CO_2 on the solution pH. More details on these apparatuses are reported by Strachan et al. [51].

The chemical durability of the ^{238}Pu-bearing ceramics was tested in solutions with a pH value of 2. Although acidic conditions will not prevail in prospective geologic repositories, pH 2 solutions allow us to avoid solubility limitations for Gd, Ce, Pu, and U. Further, we show in this report, as we have in the past [52], that there is a weak dependence of the dissolution rate on pH. Therefore, at worst, the forward dissolution rate on pH 2 is about a factor of 10 higher than the forward dissolution rate at neutral to slightly alkaline pH values.

Aliquots of effluent solution, whether from the titanium or the Teflon SPFT apparatus, were routinely checked to assure that pH control was maintained during the experiment. Other aliquots were reserved for radiochemical assay with counting techniques. Gamma energy analysis (GEA) was used to analyze for ^{239}Pu, ^{238}Pu, ^{240}Pu, ^{241}Pu, and ^{241}Am in aliquots of the effluent solution. The remainder of the periodically collected effluent was acidified ($pH < 2$) with high-purity nitric acid and analyzed for Ce, Gd, Hf, Mo, ^{239}Pu, Ti, and mass-238 species concentrations with inductively coupled plasma-mass spectroscopy. 'Mass-238' species include ^{238}U and ^{238}Pu, which we assumed constituted the total of species of mass-238. Concentrations of ^{238}U were determined by subtracting the concentration of ^{238}Pu determined with counting methods from the mass-238 species. Concentrations of Ti in effluent solutions from the titanium reactor experiments were not determined. Concentrations of Al and Ca in the solutions from the tests with Pu-bearing ceramics were determined with optical emission spectroscopy methods. This technique was not used for solutions from tests with ^{238}Pu specimens because the optical emission spectrometer was not set up for the analysis of highly radioactive solutions.

Typically, three blank solutions were drawn before the specimen was added to the reactor. The blank solutions were analyzed for background concentrations of elements of interest and, together with analyses of staring solution aliquots, assured us that contamination from previous experiments was not a factor. Blanks, which were set up identically to the other reaction cells, but without a test specimen, were used to monitor the Mo in the starting pH-buffered leach solutions. Through separate testing, we determined that one of the minor contaminants in the THAM was Mo. Analyses of the solutions from the blanks showed that the concentrations of Mo remained relatively low, but increased as water evaporated from the reservoir under flowing nitrogen. In most cases, reservoir bottles were exchanged before significant evaporation occurred. Any slight rise in background Mo concentrations was recorded. These concentrations dropped to near detection level (~0.10 μg/L) after the solution was changed. The concentration of Mo from the blank was subtracted from the Mo concentration in the effluent solutions. Because a significant fraction of the dissolved Mo sorbs on the alteration product anatase at pH values below 5 [39], no Mo results are shown for the experiments in which the leachant has a pH of 2.

To assure that the dissolution rate we measured was the forward rate for each ceramic type, we varied the solution flow rate (q) and the specimen surface area (S) until the dissolution rate was independent of q/S. Values of q/S were achieved by flow rate or surface area or both. We measured the dissolution rates of both monolithic and powdered specimens. The computation of dissolution rates and associated uncertainties has been discussed elsewhere [53] and is not repeated here.

We were also concerned about the use of Ti vessels when testing titanate ceramics. With the Ti vessels, we are unable to report the Ti concentration in solution. Therefore, we tested one ^{239}Pu-bearing specimen in both the Ti and Teflon apparatuses. Because the solubility of anatase is very low, the solutions were saturated with respect to anatase, irrespective of which vessel was used in the test. A comparison of these results in combination with the rest of the test results allows us to eliminate the vessel material as affecting the dissolution of these ceramic materials.

In the results shown below, we have assumed that the dose from the ^{238}Pu contained in each specimen is averaged over the entire specimen even though the distribution of the ^{238}Pu among the phases present is not necessarily uniform. Because we lacked the analytical tools to determine the compositions of the constituent phases and the Pu distribution, we were forced to assume an average distribution. The dose, reported in α/g, was calculated from the half-life of ^{238}Pu(87.7 y), the ^{238}Pu content of each specimen, and the time since making or resintering the specimens.

3. Results and discussion

3.1. Photographs

The specimens were produced as right circular cylinders. The pressing of these specimens was not optimized, so some edge chipping was observed. A picture from above of a typical specimen, in this case P1, is shown in Fig. 1. The defects shown in this specimen are typical for most of the specimens.

3.2. Density measurements

3.2.1. Helium pycnometer results

3.2.1.1. P1 specimens. Two sets of results are discussed here. One set is from the original P1 specimens and the other from the specimens that were resintered at 1350 °C to remove 2-years of accumulated radiation-induced damage. Results from the original and resintered specimens stored at 20 °C are shown in Fig. 2. The 'true' density of the ^{239}Pu-bearing specimens is constant over approximately 1350 days; the measurement at 199 days is likely an outlier. A starting 'true' density of 5.531×10^3 kg/m^3 is 92% of theoretical density (6.008×10^3 kg/m^3). Although the shape of the curves from the ^{238}Pu-bearing specimens is similar, the density of the resintered specimens changed much more rapidly with increasing dose than the original. This is probably a result of the resintering process, which likely led to some restructuring of the microstructure. The density results were fit to the equation

$$\rho = \rho_s + b\exp(-ct), \tag{1}$$

where ρ is the density, ρ_s is the density at saturation, b is the difference between the initial and the asymptotic (saturation) value of ρ and c is related to the damage volume per alpha decay [16]. For this fit, the values are $\rho_s = 5.156(9) \times 10^3$ kg/m^3, $b = 0.38(1) \times 10^3$ kg/m^3, and $c = 0.0042(5)$ d^{-1} (Table 2). More significant figures are shown in the figure to allow the reader to reproduce our results more accurately. For the original P1-238 specimens, the density changes appear to have saturated at a density of 5.16×10^3 kg/m^3 – a decrease of 6.9% – and a dose of about 2.8×10^{18} α/g. The change in the density for the resintered specimens did not saturate or come sufficiently close for us to apply Eq. (1) to the data. The rate of change in density for the resintered P1-238 specimens is $-8.32(56) \times 10^{-4}$ kg/(m^3 d) in the linear portion of the data in Fig. 2. We surmise that the density would saturate between 5.0 and 5.1×10^3 kg/m^3 for an 8 –10% decrease in the density.

Fig. 1. A picture of a typical P1-238 or PB1-238 specimen (color wheel in the background for true color rendition). (For interpretation of the references in color in this figure legend, the reader is referred to the web version of this article.)

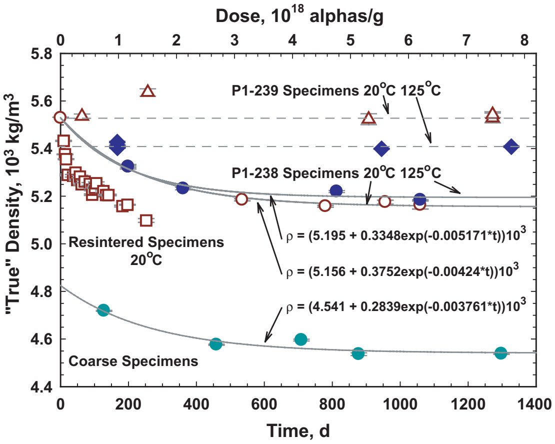

Fig. 2. A graph showing the results of the 'true' density measurements for the P1-238 and P1-239 specimens stored at 20 and 125 °C and the coarse specimens.

Results from the density measurements of the specimens stored at 125 °C are shown in Fig. 2. No specimens that had been stored at 125 °C were resintered and stored again at 125 °C. From these data, it is unclear if the density change has saturated. However, fitting the data to Eq. (1) suggests that the density ($5.195(9) \times 10^3$ kg/m^3) at saturation is the same within experimental uncertainty as the density at saturation of the original specimens stored at 20 °C (Fig. 2).

As has been reported previously [54,55] there are changes to the pyrochlore (PI-238) specimens stored at 250 °C that were not observed in the specimens stored at 20 °C. These changes appear to be manifest in the density changes as seen in Fig. 3 and will be discussed in Section 3.4. While the density of the resintered specimens that were originally stored at 250 °C has the same starting value of about 5.4×10^3 kg/m^3, the densities change linearly with time and coincide with the densities of the original specimens (Fig. 3). The rate of change in

Table 2
Summary results from the ‘true density’ measurements on P1-238 and PB1-238 specimen

Specimen	Temperature, °C	Saturation density, ρ_s, 10^3 kg/m^3	b, 10^3 kg/m^3	c, d^{-1}	Decrease, %	Saturation dose, 10^{18} α/g
P1	20	5.156(9)	0.38(1)	0.0042(5)	6.9	2.8
	125	5.195(16)	0.34(2)	0.0052(10)	6.1	2.1
	250	4.789(120)	0.62(12)	0.00090(27)	11.5	15
P1 Coarse	20	4.541(29)	0.28(8)	0.0038(24)	5.8	2.8
PB1	20	5.060(20)	0.72(8)	0.0061(15)	12.5	2.5
	125	5.096(32)	0.54(3)	0.0029(6)	9.6	4.6
	250	5.240(32)	0.46(7)	0.011(5)	8.1	1.1

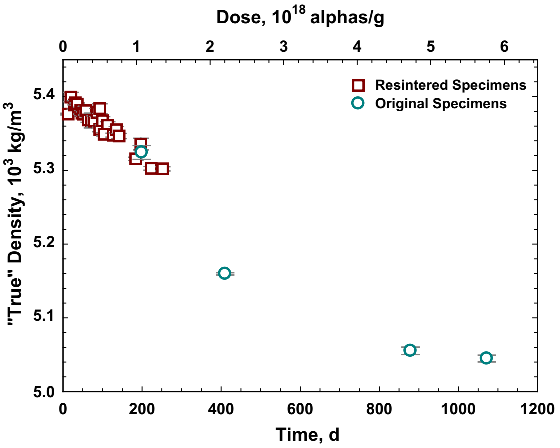

Fig. 3. A graph showing the change in the ‘true’ density of P1-238 with time for specimens stored at 250 °C.

the density is $-3.88(28) \times 10^{-4}$ kg/(m^3 d), which is slower by about a factor of two than the change shown in Fig. 2 for the specimens stored at 20 °C. The coincidence of th data from the resintered specimens with the data from the original specimens suggests that the resintered density should decrease to about 5.1×10^3 kg/m^3 after about 800 days (−5.5%).

‘True’ densities were also measured for the coarsened microstructure P1 specimens (Fig. 2). The data from the ^{238}Pu-bearing specimens were fit to Eq. (1). A 5.8% decrease in the ‘true’ density of the ^{238}Pu-bearing specimens is in good agreement with the 6.9% decrease noted for the original specimens also stored at 20 °C. These data and the data from the specimens stored at 125 °C suggest that the critical temperature is greater than 250 °C.

Based on the calculated starting densities, prolonged sintering (100 h extra sintering of original specimens at the time they were prepared) of these materials appears to reduce the ‘true’ density, 2% for the ^{239}Pu-bearing specimens and 13% for the ^{238}Pu-bearing specimens.

3.2.1.2. PB1 specimens. Results from the measurement of the ‘true’ density of the original PB1 specimens are shown in Fig. 4. At saturation, the densities are 5.06×10^3, 5.10×10^3, and 5.24×10^3 kg/m^3 at 20, 125, and 250 °C, respectively. We obtained the starting density of the PB1-238 specimens by extrapolating the data back to the start with the use of Eq. (1) and obtained an average starting density of $5.67(1) \times 10^3$ kg/m^3. Relative to this extrapolated value, the densities at saturation represent decreases of 12.5%, 9.6%, and 8.1% for the PB1-238 specimens stored at 20, 125, and 250 °C, respectively. Although the experimental error is low, we feel that the low density determined at about 225 days for the specimens stored at 125 °C is an outlier and should be ignored as are the data for the specimens stored at 250 °C at about 275 days. Overall, the data seem to indicate that the radiation-induced changes to the ‘true’ density have saturated after 2×10^{18} to 4×10^{18} α/g (an average dose for the whole specimen). The low values for the density of the specimens stored at 250 °C and about 275 days suggest that we were having problems with the determination at that time. However, we did not know the measurements were in error until subsequent measurements were made.

In Fig. 5, we show the results for the ‘true’ densities of the resintered PB1-238 specimens stored at 20 °C and 250 °C after resintering; the same temperature at which they were stored before resintering. No resintered specimens were stored at 125 °C. After an apparent delay of about 10 days, the ‘true’ density drops exponentially as do the densities of the original specimens. If we take out the apparent 10-day delay and fit the resulting data to Eq. (1), we project a value of $5.68(2) \times 10^3$ kg/m^3 as the starting density, which is similar to the density of the PB1-238 specimens and the extrapolated starting density for the original specimens discussed above, $5.67(1) \times 10^3$ kg/m^3. Using the projected value and asymptotic value of 5.03×10^3 kg/m^3, we calculate an 11.4% decrease, in good agreement with the change in the ‘true’ density of the original PB1 specimens at 20 °C. It is unclear from these data why there should

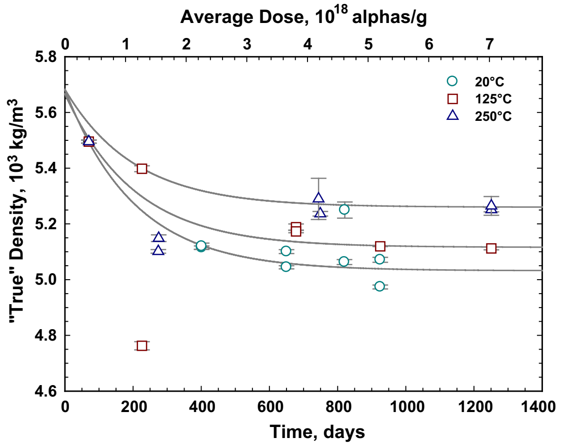

Fig. 4. Results from the measurement of the 'true' density of PB1-238 specimens stored at 20, 125, and 250 °C.

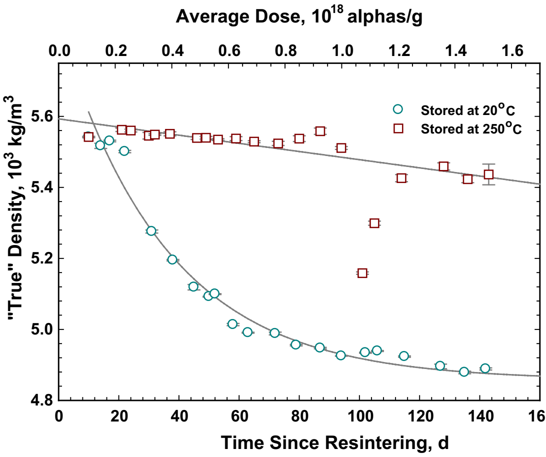

Fig. 5. The variation of the 'true' density of the PB1-238 specimens that were resintered and stored 20 and 250 °C.

be a 10-day induction period. However, Weber et al. [14] and Clinard [56] have seen densification on annealing of the accumulated damage. If the data for the specimens stored at 20 °C are extrapolated to zero time by use of Eq. (1), a starting density of 5.9×10^3 kg/m^3 is obtained (implying a 17% decrease in density upon amorphization). This suggests an approximate 4% densification of these specimens over the as-prepared density of 5.65×10^3 kg/m^3 (Fig. 4). While this is a reasonable densification based on existing data, the lack of densification for the resintered specimens stored at 250 °C then needs to be explained. Excluding the two data points at about 100 days, the slope of the straight line drawn through the 'true' density data from the specimens stored at 250 °C is $-1.15(15)$ kg/(m^3 d); a slope similar to that one would calculate from the original specimens stored at 250 °C (Fig. 4). In fact, the two data sets (original and resintered) for the specimens stored at 250 °C superimpose on one another over the first 140 d, but the data sets for the specimens stored at 20 °C do not. The density after resintering (ordinate in Fig. 5) for the specimens stored at 250 °C is about the same as the density for the original specimens and suggests little or no densification of these specimens even though they were also rendered amorphous from radiation-induced damage before the damage was annealed through resintering. This result might suggest that the recovery of the damage induced at lower temperatures involves the movement of more atoms and defects, as well as the release of more energy than during the recovery processes for materials in which the damage was accumulated at higher temperatures. For the PB1-238 specimens stored at 250 °C, the slope is about three times greater than the slope observed for the P1-238 specimens stored at 250 °C ($-0.388(24)$ kg/(m^3 d)).

3.2.2. Geometric densities

3.2.2.1. P1 specimens. The measured diameters of the original ^{238}Pu- and ^{239}Pu-bearing P1 specimens are shown in Fig. 6. When the specimens were made, all had the same diameter within experimental uncertainty [10.3(1) mm]. These diameters were measured with a hand-held micrometer, hence the higher uncertainty. The measurements that were made between 200 and 400 days were made with the laser-based instrument, but for a short measurement time that resulted in higher uncertainty. No significant temperature dependence is observed. Several data points appear to result from measurement error and do not fit the trend if the majority of data, e.g., the low data at 1072 days and at 1350 days. The majority of the ^{238}Pu-bearing specimen data were fit to the equation

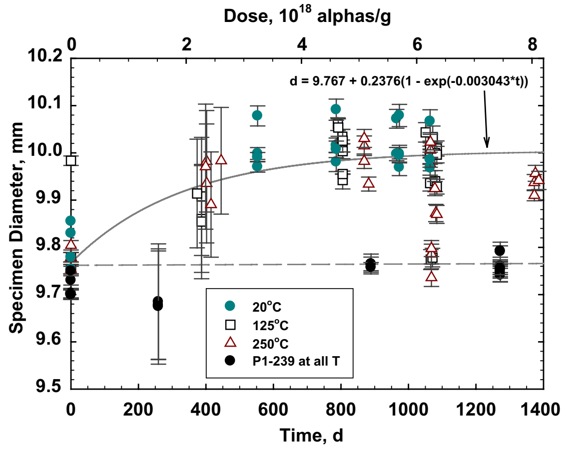

Fig. 6. The variation of the diameters of P1-238 and P1-239 specimens that were stored at 20, 125, and 250 °C.

$$d = d_0 + a(1 - \exp(-bt)), \tag{2}$$

where d is the specimen diameter, d_0 is the diameter at zero dose, a is the difference between the initial and the asymptotic (saturation) value of d, and b is related to the damage volume per alpha decay [14] and the half-life of the active isotope. The least-squares fit of the measured diameters to Eq. (2) yielded values for the variables of $d_0 = 9.767(12) \times 10^3$ kg/m^3, a = $0.23(2) \times 10^3$ kg/m^3, and $b = 0.0030(7)$ d^{-1} (Table 3). More significant figures are shown for the variables in Fig. 6 than are warranted by the uncertainties so that the reader can accurately reproduce the curves shown. Using the asymptotic value for the increase in the diameter, we calculate that the diameters swelled by 2.4% or a volume increase of 7.4%. Thus, the bulk density is calculated to decrease by 6.7%. This agrees well with the change in the density measured with the He pycnometer of 6.9% and 6.1% for the specimens stored at 20 and 125 °C, respectively (see discussion above), but not with the change at 250 °C. As will be discussed below, there are changes in crystal structure that may be the cause of this difference.

We also show the change in the diameters with time of the ^{238}Pu- and ^{239}Pu-bearing coarse P1 specimens stored at 20 °C in Fig. 7. An increase in the diameter of 2.6% is noted, indicating an increase in the specimen volume of 7.9%. Thus, the geometric density decreases by 7.3% based on the dimension increase. This compares with the decrease in the 'true' density (6.9%) discussed above for the P1-238 and the decreases in the specimens made without coarsening of the microstructure. Our values for the swelling of these materials at saturation and the saturation doses are similar to those reported in the literature [13,14,18,25]. Our data suggest marginal temperature dependence. Certainly, there is no evidence for temperature dependence in our dimensional data.

Resintering the P1-238 specimens did not significantly affect the diameters (an example is shown in Table 3). Each of the diameters are slightly different, varying by about 0.1 mm. The average shrinkage on resintering is about 1.5%, which is within the measurement uncertainty for the measurements on the original specimens is for which a hand-held micrometer was used. In Fig. 8, the diameters of two of the resintered specimens are shown. Over approximately 260 days, radiation-induced

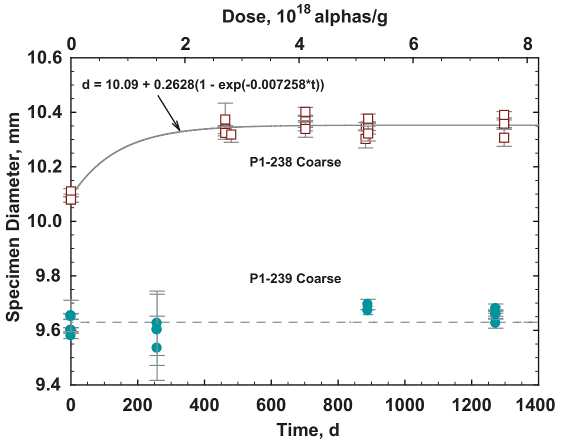

Fig. 7. The variation of the diameters of coarse P1-238 and P1-239 pyrochlore specimens stored at 20 °C.

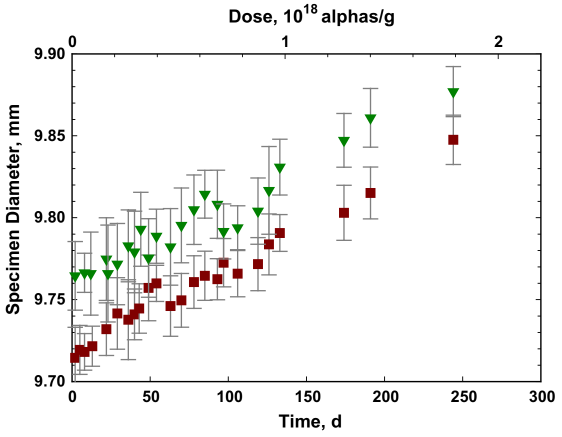

Fig. 8. A graph showing the variation in the diameter of the resintered P1-238 specimens.

Table 3
Summary diameter measurements on the P1-238 and PBl-238 specimens

Specimen	Initial diameter (d_0), mm	a, mm	b, d^{-1}	Increase, %	Density decrease, %	Saturation dose, 10^{18} α/g
Original						
P1	9.767(12)	0.23(2)	0.0030(7)	2.4	6.7	1.5
Coarse	10.09(1)	0.26(2)	0.0073(39)	2.6	7.3	1.9
PB1	10.30(2)	0.217(20)	0.0061(16)	2.1	6.1	2.6
Resintered						
P1	9.754(79)	0.16(8)	0.064(47)	1.6	4.8	2.3
PB1	9.830(19)	0.55(69)	0.0089(250)	5.6	15.1	2.5

swelling resulted in 1.1% increase in the diameter or a decrease in density of 3.3%. This compares with approximately 6% decrease in the 'true' density over the same time period. These results suggest a closing of open porosity as the individual grains swell resulting in a more rapid decrease in the 'true' density when compared with the bulk density.

3.2.2.2. PB1 specimens. The variation in the diameters of the PB1 specimens stored at 20, 125, and 250 °C is shown in Fig. 9. From the measurement of the diameters, there appears to be no temperature dependence in the radiation-induced swelling of the specimens. That is, there is no systematic difference between the observed swelling of the specimens held at ambient conditions or at 250 °C. The data were fit to the Eq. (2). These data suggest that the changes in the diameters saturate at about 2.3×10^{18} α/g (410 days) for a final diameter of 10.459(78) mm. This suggests that the diameter expanded by 2.1% for a volume expansion of 6.4% or a 6.0% decrease in the bulk density, much less than the observed decrease in the 'true' densities, which are sensitive to the amount of closed porosity. This indicates that open porosity was converted to closed porosity as the specimen swelled with increasing radiation-induced damage.

Changes in the diameters of the resintered PB1 specimens are shown in Fig. 10. These data indicate that the change is linear over the time of characterization for the specimens that were originally stored at 20 °C and stored at 20 °C after resintering. Taking the swelling of specimen 8PB1B-7 as representative of the behavior of all the PB1 specimens (Fig. 10), we calculate a slope for the linear behavior of the diameter as $2.6(3) \times 10^{-4}$ mm/d. This rate of swelling is about half of what is needed to explain the swelling observed in the original specimens shown in Fig. 9. This difference may be the uncertainty in the measurements of the original or resintered specimens, or it could reflect the changes (densification) that occurred during resintering. Similarly, the diameters of the specimens that were stored at 250 °C and stored at 250 °C since resintering also swell linearly with a slope of $1.9(2) \times 10^{-4}$ mm/d (Fig. 11). As with the original specimens, there is no significant difference in the rate of swelling between the specimens stored at 20 and 250 °C. These effects were not noted in P1 specimens. Over the 281 days (20 °C) or 325 (250 °C) days of the test, the specimens swelled about 1.1% for a calculated density change of −3.2%. This value is inconsistent with the 15.1% decrease in density determined above for the original PB1 specimens

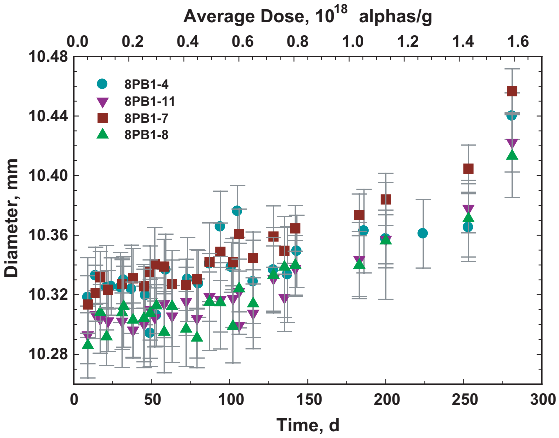

Fig. 10. The variation in the diameters of the individual PB1-238 specimens originally stored at 20 °C and stored at 20 °C since resintering.

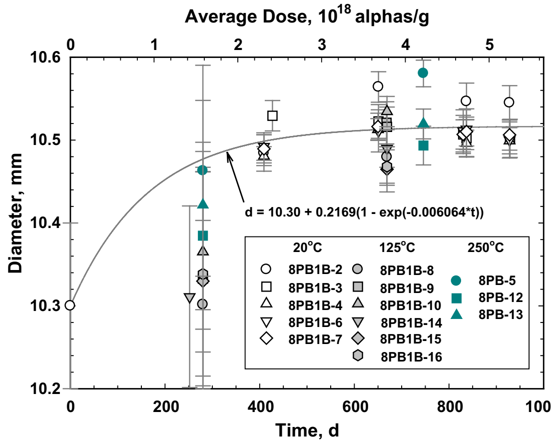

Fig. 9. The variation with increasing dose of the P1-238 specimen diameters for the original at 20, 125, and 250 °C.

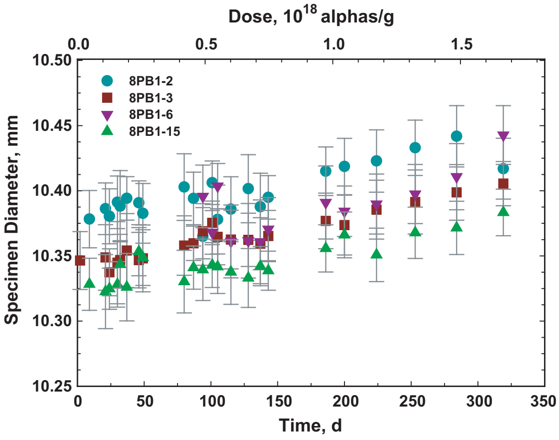

Fig. 11. The variation in the diameters of the individual PB1-238 specimens originally stored at 20 °C and stored at 250 °C since resintering.

and suggests some densification occurred during the resintering.

Because the 'true' density for the specimens stored at 20 °C changed by substantially more than what was observed from the diameters of the specimens and by more than the 'true' densities of the specimens stored at 250 °C, we conclude that some open porosity became closed porosity as the specimen swelled. At about 8–10% total porosity, the change from open to closed porosity is quite rapid with small changes in total porosity [57]. As open porosity was converted to closed porosity, there was less pore volume accessible to the He gas, so the specimen density appeared to decrease more rapidly. The effect of particle swelling might not be as important for the specimens stored at 250 °C. This would be consistent with the slightly lower rate of swelling observed for the specimens stored at 250 °C. The microscopic swelling (see the discussion below on the XRD results) results show that the expansion of the unit cell(s) of the phases in the specimens stored at 250 °C is slower than the swelling for the phases in the specimens stored at 20 °C.

Our results do not allow us to determine the critical temperature. For most data, there is no observable temperature dependence. However, we can say that at a storage temperature of 250 °C, we are below the critical temperature. Critical temperatures for these materials are generally in the range of 500–1000 K (225–725 °C) [16]. Since the temperature dependence below the critical temperature is low, we might be unable to detect it for the temperature range used here.

3.3. Scanning electron microscopy

3.3.1. P1 specimens

The SEM images of a sample from an original (fully damaged) P1-238 specimen stored at 20 °C revealed two major phases but also a series of other minor phases within the ceramic. In the back-scattered images of the phases shown in Fig. 12(A), the phase that appears dark is rutile, and the Pu- and U-bearing pyrochlore phase appears light. A spherical precipitate that appeared to contain a heavy element(s) was occasionally observed (Fig. 12(B) and (C)) within the rutile. Unfortunately, the analysis of these types of small precipitates was not possible because the beam penetration extends to too great a depth.

Hafnium that was present in the rutile component of the ceramic appeared to be at a relative level of about 5–10% (Fig. 12(D)); however, based on the contrast variations within rutile grains, it is clear that there are either compositional variations within the rutile grains or overlying pyrochlore material. With the current analysis and techniques, it is not possible to distinguish between the two possibilities.

Images of the pyrochlore regions reveal subtle contrast changes across the ceramic (Fig. 12(A)). These features were not visible in the secondary imaging mode

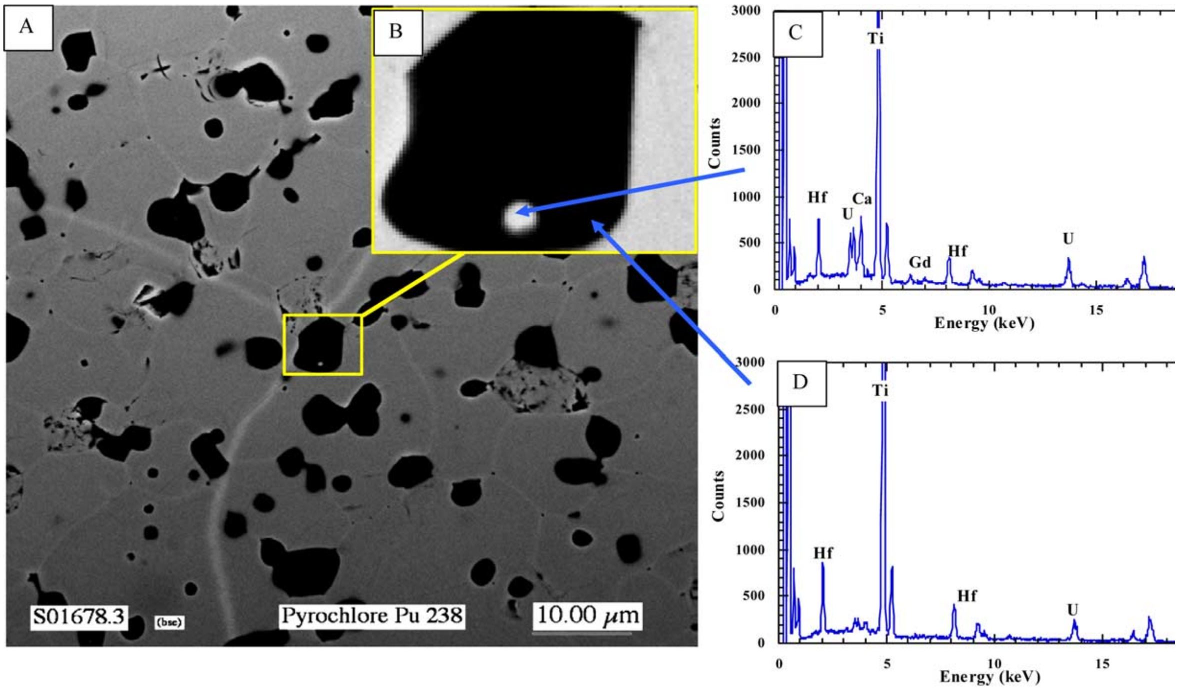

Fig. 12. (A) Backscattered electron image of grain structure from a P1-238 ceramic (stored at 20 °C; fully damaged). The insert (B) shows a Hf-bearing rutile particle with an actinide-rich inclusion as evidenced for the EDS analyses of these particles ((C) and (D)).

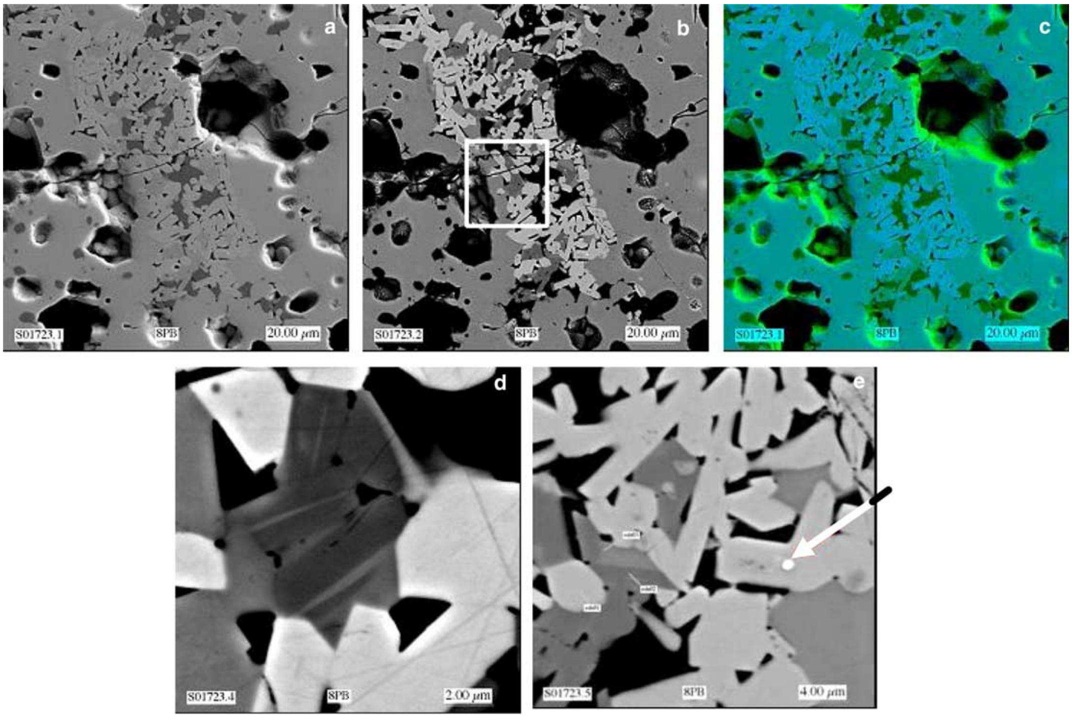

Fig. 13. An SEM photomicrograph of a fully damaged PB1-238 specimen: (a) secondary electron image, (b) backscattered electron image, (c) combined SE and BSE highlighting pores or absent grains vs mineral grains with low atomic number, (d) area within the box in (b) and (e) a small actinide-bearing inclusion.

and are therefore most likely actual compositional variations. The features were on too fine a scale to obtain accurate compositional data; however, the lighter regions appeared to be slightly enriched in Pu. It was not possible to distinguish with X-ray energy dispersive spectroscopy (EDS) analysis the reasons for this contrast variation; however, a slight oxygen deficiency and/or local densification of the phase could have produced the lightening effect. This effect was also observed delineating many of the pyrochlore grain boundaries. From the XRD results, there is evidence that phase segregation occurred at a fine scale and that the phases have different compositions.

By maximizing contrast for the pyrochlore phase, the grain boundaries can be seen (Fig. 12(A)). The grain boundaries were marked by higher average atomic mass contrast. Again, the compositional variations were not apparent from the EDS. These variations could be from compositional variations in either an increase in the heavy elements (Pu and U) or a decrease in the lighter elements (Ca and O). We could not distinguish between the possibilities.

3.3.2. PB1 specimens

The PB1-238 ceramic sample, an original specimen stored at 125 °C and fully X-ray amorphous, considered of three major phases: pyrochlore, zirconolite, and rutile. Minor actinide oxide inclusions were also observed in the material (see Fig. 13(a)–(e)). Fig. 13(a)–(d) shows the presence of crystals containing heavy elements in the ceramic. By combining the secondary electron (Figure 13(a)) and backscattered electron (Fig. 13(b)) images, it is possible to discriminate between pores and the rutile phase (Fig. 13(c)). The rutile phase exhibits low contrast in backscattered electron imaging mode. In Fig. 13(b), black regions cannot be readily identified as pores or phases, but in Fig. 13(c), some of these black areas are clearly a phase. The box area is shown in detail in Fig. 13(d). Fig. 13(d) shows evidence for lamellae structures within the pyrochlore grains. The backscattered electron image shows microstructure consistent with zirconolite intergrowths within the pyrochlore phase, similar to that reported by Buck et al. [58]. The euhedral pyrochlore grains (grey and white) would have solidified before the anhedral rutile phase (black). The marks on the phase that appear white are polishing scratches on the ceramic surface. In Fig. 13(e), a small actinide inclusion can be seen. This is marked by an arrow in the figure. This indicates that during cooling, not all the actinides could be incorporated into the main phase. Identification of the ceramic phases with EDS is not precise. In Fig. 14(a) and (b), spectra from pyrochlore and

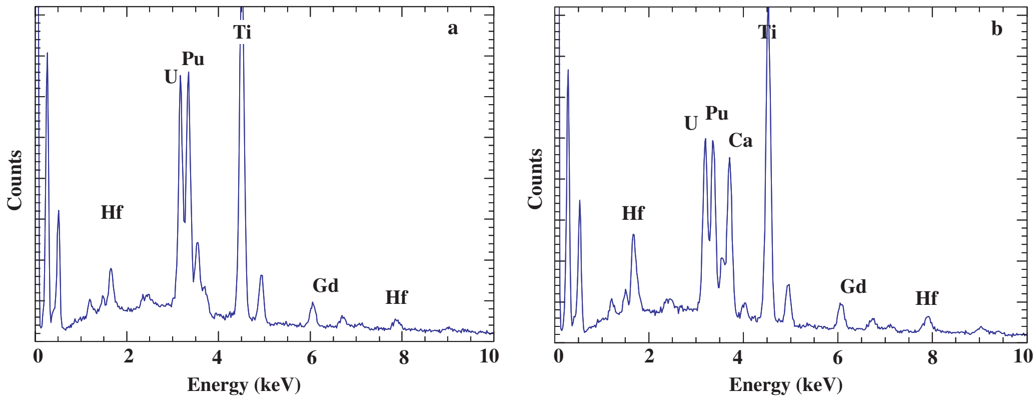

Fig. 14. Energy dispersive spectra from the PB1-238 specimen shown in Fig. 13 showing typical spectra for (a) pyrochlore and (b) zirconolite.

zirconolite, respectively, are shown. The zirconolite composition had a higher concentration of Hf and Ca compared to the pyrochlore phase.

3.4. X-ray diffraction

3.4.1. PI specimens

The results from the XRD analyses of the P1 specimens are discussed in this section and summarized in Table 4. As with the other measurements, there are results from the original and resintered specimens. The results from the original P1-238 specimens stored at 20 °C are shown in Fig. 15. The diffraction patterns are not to scale; they have been scaled for display purposes. These results indicate that by the time the first measurement was made, a large amount of radiation-induced damage had occurred. Although the diffraction peaks are labeled 'P' for pyrochlore (Fd3m), many of the diffraction peaks that define the pyrochlore symmetry were at low enough intensity that the refinement of the parameters proved difficult. Somewhere between fully crystalline and fully amorphous, the diffraction peaks begin to represent diffuse scattering rather than true Bragg diffraction [59]. However, we continued to analyze the diffraction patterns as if the diffraction represented the crystalline material that was present in the specimen. Indexed with the major peaks in the pattern, the unit cell is calculated to be 1.015–1.021 nm, depending on the amount of dose.

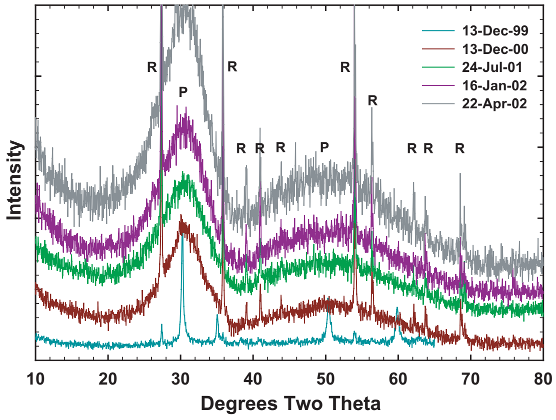

Fig. 15. Results from the XRD analyses of the original P1-238 specimens (P = Pyrochlore; R = Rutile; the patterns are in reverse order of the legend).

A compilation of the XRD patterns from the resintered P1-238 specimens is shown in Fig. 16 for the specimens that had been stored at ambient conditions before and after resintering. In Fig. 16, the shift to larger unit

Table 4
Summary XRD results from the P1-238 and PB1-238 specimens

Specimen	Temperature, °C	a_0, nm	b, nm	c, d^{-1}	Increase, %	Decrease in cell density, %	Saturation dose, 10^{18} α/g
P1	20/20	1.015(3)	0.0126(6)	0.0059(8)	1.2	3.6	2.4
	125/250	1.015(1)	0.010(1)	0.0096(16)	1.0	2.9	0.8
	250/20	1.016(5)	0.0157(12)	0.0071(14)	1.5	4.5	1.9
PB1	20	1.016(1)	0.0140(5)	0.0048(4)	1.4	4.0	2.4
	250	1.016(1)	0.0163(20)	0.0025(5)	1.6	4.7	1.9

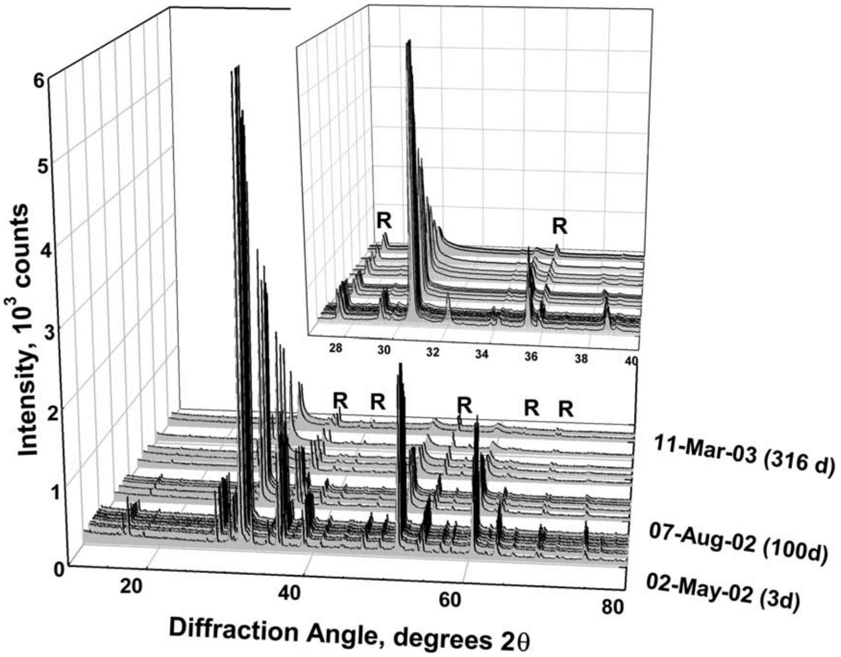

Fig. 16. Results from the XRD analyses of the resintered P1-238 specimen, showing the radiation-induced damage effects (R = Rutile).

cell sizes (smaller diffraction angle) and decrease in peak intensity can be seen. The intensity of the diffraction peaks drops rapidly over the 316 days that the data were collected. The weak diffraction peaks from the pyrochlore phase are the first to disappear, but this appears to be mainly because we were unable to perform the scans at sufficiently low speeds; had we scanned more slowly to obtain a better discrimination between signal and background, the weak peaks might have been detectable to much higher doses. As the pyrochlore becomes amorphous, it becomes more difficult to index the phase as a pyrochlore, although a characteristic (3 1 1) diffraction peak is still visible at the end of the experiment. The variation in the a_0 lattice parameter for the pyrochlore phase is shown in Fig. 17. For the data obtained after 140 days (second symbol for each data set), the lattice parameters were obtained from only the strong diffraction peaks. The data were fit to the equation

$$a = a_0 + b(1 - \exp(-ct)), \tag{3}$$

where a is the pyrochlore lattice parameter, a_0 is the lattice parameter at zero dose, b is the difference between the initial and the asymptotic value of a, and c is related to the average product of damage rate and damage volume per alpha decay per unit cell per unit time. The results of the least-squares fit to the data are a value of a_0 of 1.015(0.3) nm and an asymptotic value of 1.027(0.9) nm at approximately 390–440 days (a dose of 2.3×10^{18} to 2.6×10^{18} α/g); consistent with the data from the original specimens stored at 20 °C. Based on the asymptotic value, the lattice parameter swells by 1.2% or the cell volume by 3.6%. These data are summarized in Table 4. The results are consistent with the macroscopic swelling discussed above. Also, since these are average doses to the specimen and there is approximately 20 mass% $Hf_{0.1}Ti_{0.9}O_2$, the actual dose to the pyrochlore phase is higher than that shown or calculated.

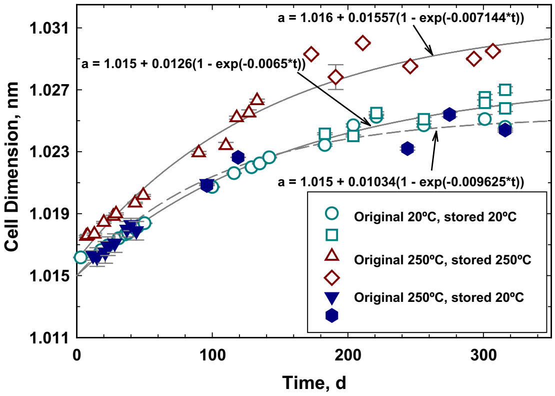

Fig. 17. The variation in the a_0 lattice parameter for the pyrochlore phase in the resintered specimen stored at 20, 250 °C, (250 °C originally), and 20 °C (250 °C originally).

While the relative intensity of the rutile peaks increases because rutile is the only remaining crystalline

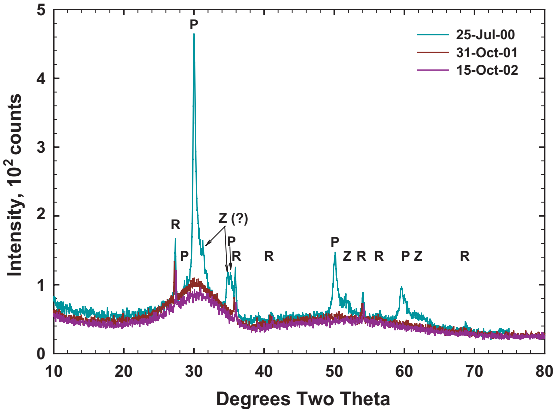

Fig. 18. Results from the XRD analyses of the P1-238 specimen stored at 250 °C since being made.

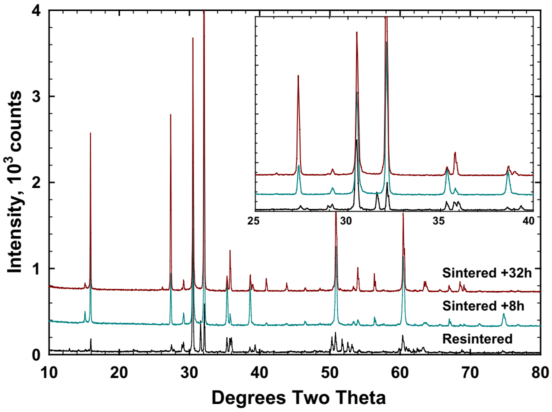

Fig. 19. Results from XRD analyses of the P1-238 specimen that had been stored at 250 °C and, after accumulating damage, was sintered again for 8 h plus an additional 24 h.

phase, there is a small shift to larger unit cell sizes (see [51]). Since there is no Pu in the rutile phase [7], the small swelling probably comes from the alpha particle damage and the small amount of recoil damage from the surrounding pyrochlore phase.

Specimens were also stored at 125 and 250 °C since being made. Since there were no significant differences between the results from the specimens stored at 125 °C and the results discussed above for the specimens stored at 20 °C, we do not discuss the XRD results for the specimens stored at 125 °C.

As with the specimens stored at ambient temperatures, the P1-238 specimens stored at 250 °C became amorphous quite quickly (Fig. 18). Although these specimens began as a mixture of pyrochlore and rutile, there was evidence for the ingrowth of a zirconolite phase (Fig. 18). By the time the specimens were examined after approximately 1 year of damage accumulation, the XRD pattern showed them to be heavily damaged (Fig. 18). In the specimen examined on 25 July 2000, we saw evidence for the presence of zirconalite that we did not see in the specimens stored at 20 and 125 °C. The peaks labeled in (Fig. 18). appear to be from zirconolite – the split peak at 35° 2θ and the high 2θ tails on the peaks at 50° and 60° 2θ. These peaks disappeared by the next examination. A selected P1-238 specimen that had been stored at 125 °C for nearly 2 years was resintered for 2 h at 1350 °C. Surprisingly, this treatment yielded a phase assemblage of pyrochlore, minor rutile, and what appear to be two zirconolites, each with different lattice parameters (Fig. 19). The two phases could be indexed as zirconolites, although there appeared to be substantial preferred orientation perhaps from the surface defects. Since the specimens stored at 250 °C from the start showed evidence for ingrowth of zirconolite (Fig. 18), it is possible that the sintering process was insufficient to return the phase assemblage to pyrochlore and rutile, but sufficient to develop the phases that formed during storage at 125 and 250 °C with the accumulated radiation damage, although they were not evident in the XRD from the original specimens. Besides the possible zirconolite peaks at 31° and 35° 2θ in the XRD shown in Fig. 18, the peaks at 50° and 60° 2θ are atypically broad and asymmetric to be only pyrochlore peaks. In the zirconolite diffraction pattern, there are groups of moderate to moderately intense peaks that occur at these diffraction angles. Therefore, the evidence is strong for the presence of zirconolite in the specimen stored at 250 °C and suggests the presence of zirconolite in the specimens stored at 125 °C even though zirconolite was not detected in the XRD from these specimens. After these data were collected, we selected one of the specimens that had been stored at 125 °C and sintered it at 1390 °C for 8 h under flowing Ar. The resulting material gave an XRD pattern that was consistent with pyrochlore, rutile, and a single zirconolite with preferred orientation (Fig. 19), possibly from the surface defects. An additional 24 h of sintering at 1350 °C resulted in a refinement of the crystalline phases, but preferred orientation remained for the zirconolite phase. These results suggest a change in the chemical makeup of the specimens, perhaps changes in the oxidation state of Pu, Ti, and U. These elements might be stabilized in these oxidation states once in the zirconolite structure.

To more clearly see the changes in the zirconolite and pyrochlore phases with increasing radiation-induced damage, three XRD patterns from suite of XRD patterns for these specimens are shown expanded in Fig. 20. In this graph, the rutile diffraction peaks are labeled. With increasing accumulated damage (time), the unit cells for the pyrochlore and zirconolite phases expand and the diffraction peaks move to lower diffraction angles. The main peaks for pyrochlore ($hkl = (222)$) and zirconolite (221) overlap at about 30° 2θ. The telltale peak for pyrochlore in these diffraction patterns is the

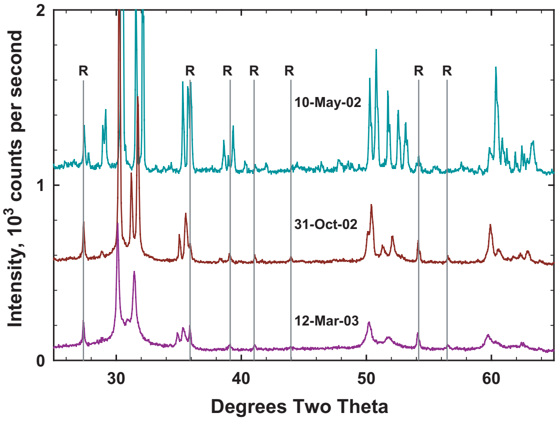

Fig. 20. Selected XRD patterns showing the effects of radiation damage on the pyrochlore and two zirconolite phases in the P1-238 specimen originally stored at 250 °C and stored at 250 °C since resintering.

peak at about 29° 2θ (3 1 1). This peak diminishes with time, but is still detectable at the end of the experiments. The ratio of the intensities, however, remains approximately the same. Because this peak is so small, it was not possible throughout the duration of the experiments to index the pattern on the pyrochlore lattice, but the pattern could be indexed with just the strong peaks. The change in the lattice parameter for the cubic cell is shown in Fig. 17. Eq. (3) was least-squares fit to the data. The values for a_0 reported in the figure are again reported to more significant figures than are warranted to provide the reader with the ability to reproduce the curves. For this fit, the values are $a_0 = 1.016(0.5)$ nm, $b = 0.016(1)$ nm, and $c = 0.007$ (14) d^{-1} (Table 4).

Changes in the zirconolite structures are evident from the patterns shown in Fig. 20. The two diffraction peaks in the range of 31°–32° 2θ are assigned to the (0 0 4) reflection from the zirconolite phase. Both Wald and Offerman [25] and Strachan et al. [54] have shown that the expansion of the unit cell in zirconolite is predominantly along the *c*-axis. Therefore, this diffraction peak shifts to lower values of 2θ more rapidly than the surrounding peaks. It is also apparent that the two zirconolites have different ^{238}Pu contents because the intensity of the peak at the lower 2θ decreases much more rapidly than the intensity of the peak at the higher 2θ (Fig. 20).

Buck et al. [58] found that zirconolite tends to exsolve from pyrochlore as lamellae. It is uncertain if these lamellae form in the materials in the work reported here, although above we mentioned this possibility in our discussion of the SEM results (Figs. 12 and 13). Putnam et al. [60] and Helean et al. [61] report that $CaCeTi_2O_7$ is metastable with respect to $CaTiO_3$ (perovskite), CeO_2, and TiO_2. The composition of the pyrochlore used in the work reported here is more complex, and evidence of low-temperature instability was not seen. However, some radiation-induced instability was noted for the pyrochlore specimens stored at temperatures above 125 °C. The nature of this instability was not investigated further in the current work. A complete explanation of the formation of zirconolite in the specimens that were resintered after having been originally stored at 125 °C and above is not possible with the results reported here.

The results from the P1-238 specimen stored at 250 °C illustrate another problem with data interpretation. As mentioned, above, the alpha dose (second *x*-axis at the top of these graphs) should be taken as an average for the entire solid. Because we do not have compositional information for each phase, we are unable to state what the alpha dose is to each phase. It is unfortunate that attempts to obtain compositional information on each phase have failed because the direct and induced X-rays generated from the radioactivity result in a high background in the scanning electron microscope. Very small samples would have been needed, and a transmission electron microscope was unavailable in which these highly radioactive, alpha-bearing samples could have been examined.

Since the phase assemblage changed when the specimens that had been stored at 250 °C were resintered, selected specimens were also stored at ambient conditions after resintering so that the data could be compared. The family of XRD patterns for one of these specimens looks similar to that shown in Fig. 16 from the specimens that were stored at 250 °C after resintering, and so, the data are not presented here. However, the details of the changes to the pyrochlore unit cell are different and are shown in Fig. 17. These results indicate that the radiation-induced damage effects saturate at about 2×10^{18} α/g based on the least-square fit of Eq. (3) to the data. This fit results in the values for $a_0 = 1.015(0.4)$ nm, $b = 0.010(5)$ nm, and $c = 0.0096(16)$ d^{-1} (Table 4). These specimens become amorphous more rapidly than the specimens stored at 250 °C. This is expected for the specimens of the same sample stored at 250 °C after resintering because of the higher storage temperature after resintering. The rate may be higher than the rate for the specimens originally stored at 20 °C and stored at 20 °C after resintering because the ^{238}Pu content is higher in the pyrochlore phase relative to the zirconolite phases and relative to the P1-238 specimen discussed above (Fig. 17). It may also be the result of a composition change that occurred with the phase separation between the pyrochlore and zirconolites. Interestingly, the value for a_0 for the pyrochlore phase in all three materials immediately after sintering is the same, 1.015, 1.016, and 1.015 nm (Fig. 17).

Average interatomic distances can be extracted from the XRD patterns from the original specimens. The maxima at about 30° and 50° 2θ result from the metal–metal and metal–oxygen distances, respectively. The Jade program (MDI, Livermore, CA) was used to fit these broad peaks and obtain the position of the two amorphous maxima in five P1-238 specimens (four pyrochlore and one coarse pyrochlore). The average value for the metal–metal distance is 0.291(5) nm, and the metal–oxygen distance is 0.175(5) nm. These distances are similar to those found in natural pyrochlore by Lumpkin et al. [35] with the TEM, but shorter than the those reported in the $Gd_2(Ti_{1-y}Zr_y)_2O_7$ system by Hess et al. [43], who used X-ray absorption spectroscopy.

3.4.2. PB1 specimens

In this section, we report the XRD results from the PB1 specimens that were made to represent the formulation used in the Plutonium Immobilization Plant because the Pu feed stream was expected to contain other elements. As in the other sections above, we discuss the results from original specimens and from the resintered specimens. In this section, we discuss the XRD results, which are summarized in Table 4. The results from the original PB1 specimens stored at 20 °C are shown in Fig. 21. The XRD pattern (October 1999) is consistent with the presence of four phases: pyrochlore, brannerite, zirconolite, and rutile. The rutile phase remains crystalline as the other phases become amorphous, and hence, the relative intensities increase. As can be seen from the XRD patterns, the ceramic becomes amorphous quickly with the pyrochlore and brannerite peaks becoming broader and the intensities of most peaks becoming less than the background before the same happens to the zirconolite component.

After the PB1 specimens were resintered, the XRD patterns were compared, and the results are shown in Fig. 22. These patterns show that the phase assemblages were the same; there is some preferred orientation in the ^{239}Pu-bearing specimen perhaps from the surface defects. This is evident in the different intensity of some peaks and the extra peak at about 16° 2θ.

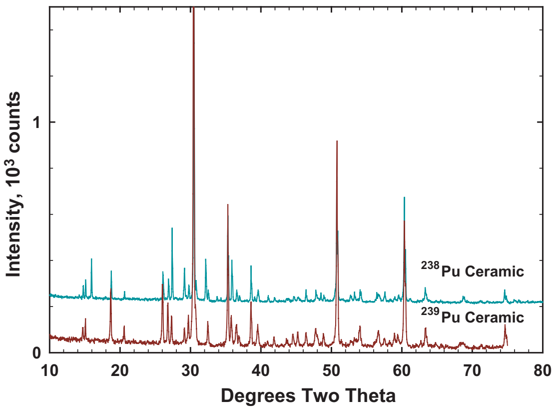

Fig. 22. A comparison between the XRD patterns of the PB1-238 and PB1-239 specimens.

Radiation-induced changes to the crystal structures in the resintered PB1-238 specimen are shown in Fig. 23. Although the pyrochlore, brannerite, and zirconolite phases undergo radiation-induced change, the changes are different than those observed in the other materials characterized in this project [43,44,48] and other studies. The diffraction peak at 36° 2θ (the [004] peak) shows that the zirconolite phase, while becoming amorphous, does not exhibit lattice-parameter changes. There is a rutile peak that falls at the same diffraction angle, so the intensity of this peak is dominated by the rutile contribution at high alpha dose. At the same time, the pyrochlore phase (peak at 35° 2θ) becomes amorphous with a significant increase in the lattice parameter. This

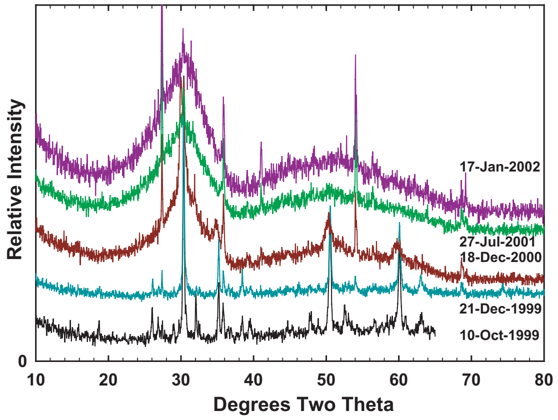

Fig. 21. X-ray diffraction patterns from the original PB1-238 specimens stored at 20 °C.

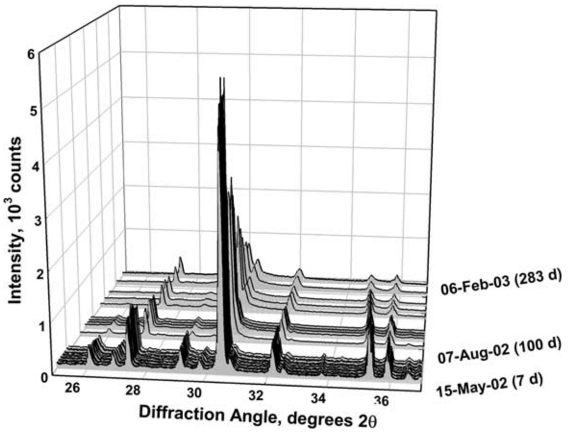

Fig. 23. A set of XRD patterns showing the effect of radiation-induced damage on the crystal structures of the phases in the PB1-238 specimens.

effect is also seen at 30° 2θ where the diffraction peak from zirconolite and pyrochlore occur initially at nearly the same value. However, with increasing dose, a separation develops between the two while both decrease in intensity and become broader. While other authors [25] and we [51,54] have shown that the predominant change to the zirconolite unit cell is along the *c*-axis, we do not see it in this material. The [0 0 4] diffraction peak at 32° 2θ remains at the same value for the duration of the experiment, although the peak becomes broader and less intense. It has been noted that radiation-induced changes to the crystal structure depend sometimes strongly on phase composition. Our results suggest that the zirconolite phase, while still containing significant concentrations of ^{238}Pu (probably >5 mass%) after resintering, has a different composition than in the original specimen (Fig. 23).

To further illustrate the changes in the crystal structures in PB1-238, we show the changes to the lattice parameters with increasing time or damage. In Fig. 24, we show the changes to the pyrochlore phase in the resintered specimen. For the data obtained after 140 days, the diffraction patterns were fit to the pyrochlore cell and to just the strongest peaks in the pattern. The data were fit to Eq. (3). The results of the least-squares fit to the data are a value of a_0 of $1.016(6\times10^{-5})$ nm and an asymptotic value of $1.031(4\times10^{-4})$ nm at approximately 675 days (an average dose of 3.82×10^{18} α/g) – approximately twice as long as the experiments with the resintered specimens were carried out. Based on the asymptotic value, the lattice parameter swells by 1.5% or the cell volume by 4.6%.

Although not shown here, there are variations in the lattice parameters, including cell angle, for the brannerite phase in the PB1-238 specimen. Up to 100 days (0.57×10^{18} α/g), there are slight increases in the a_0 and b_0 lattice parameters and decreases in the c_0 and β parameters. After 100 days, the diffraction pattern becomes difficult to refine; hence, the errors in the determinations increase. Over the first 100 days. The volume of the brannerite cell swelled by 0.2%. This small amount of swelling may reflect the fact that little, if any, Pu is in the brannerite. Pure Pu-brannerite has not been made in 100% yield [62] and has been found to be entropy stabilized at high temperature [36]. Ebbinghaus et al. [63] determined that the presence of actinides in the titanate ceramic increased the yield of pyrochlore with brannerite as the major impurity. When no actinides were present, no brannerite formed. Helean et al. [61] conclude that the presence of as much as 30 mass% brannerite in the ceramic does not significantly decrease the thermodynamic stability of the ceramic. The marginal thermodynamic stability of brannerite containing Pu may also explain its sensitivity to radiation-induced damage. Hence, the small amount of observed swelling may be consistent with the observation that the brannerite phase becomes amorphous at quite low average radiation-induced damage, whether it arises from a small amount of Pu in the phase or from radiation-induced damage from surrounding Pu-bearing phases.

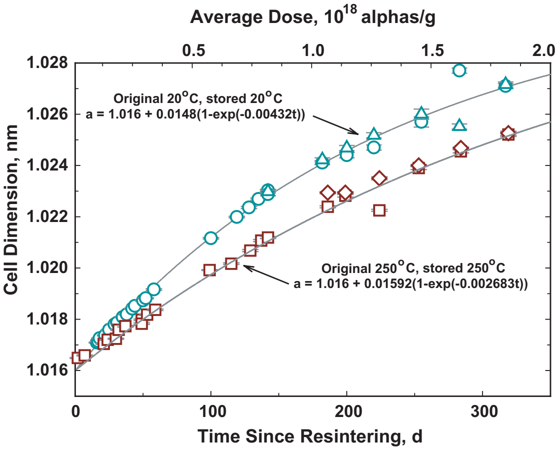

Fig. 24. The change in the lattice parameter (a_0) for the pyrochlore phase in PB1-238 specimens stored at 20 °C (originally at 20 °C) and 250 °C (originally at 250 °C).

Zirconolite, the third phase in the PB1-238 ceramic, also undergoes small changes in lattice parameters and cell angle (see [51]). However, the changes in the a_0 and b_0 axes are in opposition with a_0 increasing 2.6% and b_0 decreasing 0.75%; β also decreased by 0.84%. No significant change in c_0 was observed. The net result is an overall increase in the cell volume of 0.27%. The insensitivity to radiation-induced swelling along the *c*-axis is much different than what has been observed in the past for zirconolite [25,51,54]. The volumetric swelling of the unit cell is less than the values reported by Clinard et al. [10,31], suggesting that here is much less ^{238}Pu in this zirconolite than the pure-phase $Ca^{238}PuTi_2O_7$ used in Clinard's studies.

Although the transformation of zirconolite to an amorphous phase in ion-beam irradiation studies is reported to progress through pyrochlore [26], there is little evidence of that progression in our data or previous data on ^{244}Cm-bearing zirconolite [14]. Zirconolite is more resistant to damage than the pyrochlore in these materials. Thus, if zirconolite transforms to pyrochlore, one would expect the characteristic line at about 29.5° 2θ (the (3 1 1)) should become stronger in the diffraction patterns. The data from the P1-238 specimens show that this characteristic line remains in the pattern until a substantial amount of radiation-induced damage has occurred and appears to be at least as strong as it appears in the patterns from the PB1 specimens. Since the intensity of the (3 1 1) peak decreases similarly to the intensity of the same peak in the P1-238 specimen, the data presented in the patterns shown for both

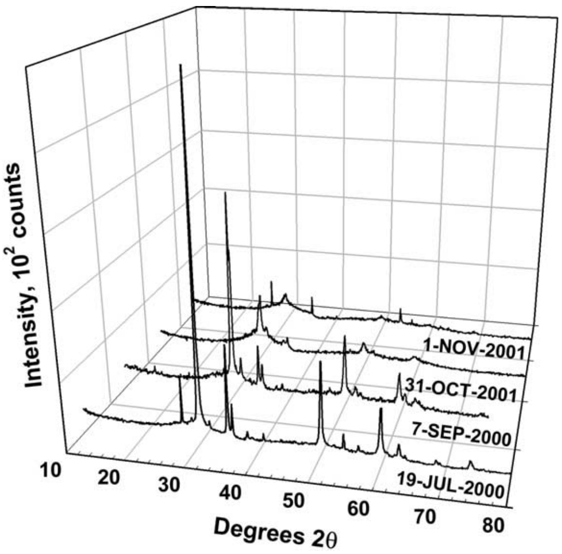

Fig. 25. A series of XRD patterns taken at various dates from the original PB1-238 specimens stored at 250 °C).

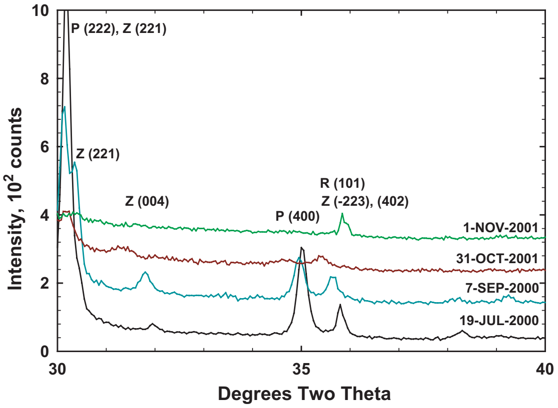

Fig. 26. An expanded view of selected XRD patterns from the original PB1-238 specimens stored at 250 °C) (P = Pyrochlore, R = Rutile and Z = Zirconolite).

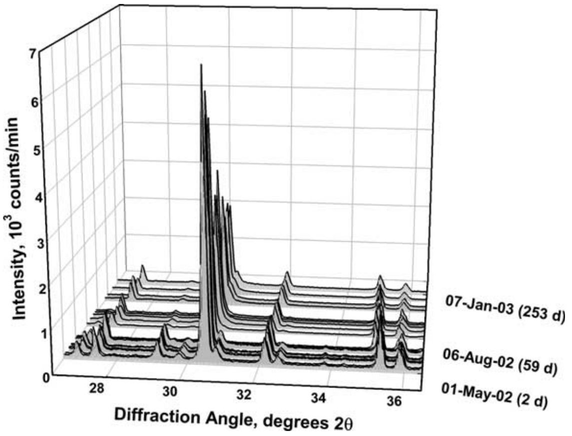

Fig. 27. A series of XRD patterns from PB1-238 specimens that were stored at 250 °C before and after resintering.

the specimen stored at 20 and 250 °C (see below) are inconsistent with zirconolite transforming to pyrochlore. We came to the same conclusion with respect to zirconolite [51].

Results from the XRD studies of the original PB1 specimens stored at 250 °C are shown in Fig. 25. Although the specimens were made in October 1999, the first diffraction pattern of the specimens stored at 250 °C was in July 2000. By this time, substantial radiation-induced damage had occurred. Although the specimens produced for this study were produced as a single batch and, hence, should have contained four phases, by the time these specimens were characterized, the brannerite phase appeared to have become amorphous. Contrary to what we saw with the specimens stored at 20 °C, the zirconolite in these specimens expands predominantly along the *c*-axis (Fig. 26). In Fig. 26, there is overlap between the rutile and zirconolite peaks. The (0 0 4) peak has a starting position of about 34° 2*θ*, and it shifts toward smaller 2*θ*, values with increasing damage, eventually disappearing. As damage accumulates in the pyrochlore and zirconolite phases, the main peaks at 30° 2*θ*, separate (September 2000 in Fig. 26). Both degrade to an amorphous maximum by November 2001 with only rutile as the remaining crystalline phase. This is consistent with the XRD patterns from the resintered specimens (Fig. 27), where brannerite is observed to become amorphous after about 100 days (peaks at 27.2° and 29°–30° 2*θ*, as examples).

As in the originally prepared specimens, the resintered specimens have four phases present: brannerite, pyrochlore, rutile, and zirconolite (Fig. 27). A much different result was found for the P1-238 specimens where two zirconolite phases were found in the specimens that were originally stored at 125 °C before resintering. As noted above, brannerite appears to be very susceptible to radiation-induced damage and becomes amorphous quickly (diffraction peaks at approximate positions of 26.8°, 29.8°, and 31° 2*θ*, as examples, see Fig. 27). Pyrochlore and zirconolite remain crystalline for the duration of the experiment, although the ingrowth of damage is evident. The effect on the lattice parameter for the pyrochlore phase is shown in Fig. 24. A least-squares fit of the data to Eq. (3) was used to draw the curve shown in Fig. 24. The initial value for a_0 is the same as for the specimens stored at 20 °C, even though these specimens had been stored at 250 °C before resintering. The asymptotic value for *a* is 1.033(1) nm, which is the same as the asymptotic value determined from the 20 °C specimen. However, the time that it takes to approach the final value is 1200 days, 1.8 times longer than at 20 °C. Since the value for c in Eq. (2) is related to the damage volume per decay event, these results suggest that the decay volume per event is about 1.6 times less than at 20 °C. A smaller relative damage volume is reasonable at the higher temperature since thermally activated recovery processes promote annealing of some damage in the collision cascade.

We observed variations in the lattice parameters a_0 and c_0 and the cell angle β for the brannerite phase in the PBl-238 specimens stored at 250 °C (see [51]). The b_0 lattice parameter does not change significantly within the error of the determination.

Variations in the lattice parameters for the zirconolite phase in the PBl-238 specimen were also observed. These data were consistent with the data from the specimen stored at 20 °C discussed above, but inconsistent with earlier results where the major change to the zirconolite unit cell was swelling along the c-axis [25,51,54]. Most of the variation in the zirconolite unit cell comes from the changes to a_0 and β; there is almost no change in b_0 (see [51]).

3.5. SPFT results

3.5.1. P1 specimens

Fig. 28 illustrates the release rate of Gd from the P1-238 specimen. After approximately 5 days, the release of Gd becomes constant with respect to time. At pH 2, Gd behaves as an indicator of the matrix dissolution, and these results yield a steady-state dissolution rate of $2.7(6) \times 10^{-4}$ g/(m^2 d), Fig. 29(a) and (b) shows the concentrations of ^{238}Pu and U over the duration of the experiment. While the release of ^{238}Pu reaches steady-state, the U concentrations do not. A reasonable dissolution rate can be extracted from the average concentration of ^{238}Pu from day 7 to 10 and is $8.2(6) \times 10^{-5}$ g/(m^2 d). The release of U appears to decrease linearly, although there is a lot of noise in the data. A rate of $8.9(20) \times 10^{-4}$ g/(m^2 d) can be estimated from the last three data points. In summary, the release of Gd to solution best represents the dissolution rate of the pyrochlore specimen with the release of Pu a factor of 3 lower. Therefore, even it pH 2 and 85 °C, the release of Pu is very low.

The dissolution rate of the P1-238 specimen can be compared to that of non-radioactive specimens [65] (Fig. 30). These data indicate that forward dissolution rates (constant rate with increasing (q/S) appear to occur at $\log_{10}(q/S)$ values of >-7. The forward dissolution rate for the ^{238}Pu-bearing pyrochlore specimen that had been resintered plots close to the forward dissolution rates of the non-radioactive specimens. Significantly, the data for all of the ^{238}Pu-bearing specimens (titanium vessels) plot amongst the data for the non-radioactive specimens (Teflon vessels). These data suggest that radioactive and non-radioactive specimens dissolve at the same rate, once q/S is taken into account. The data for the monolithic specimens are about a factor of 3 greater than the corresponding data from the powdered specimens. We believe this may be a result of the porosity of the specimen and the fact that we use

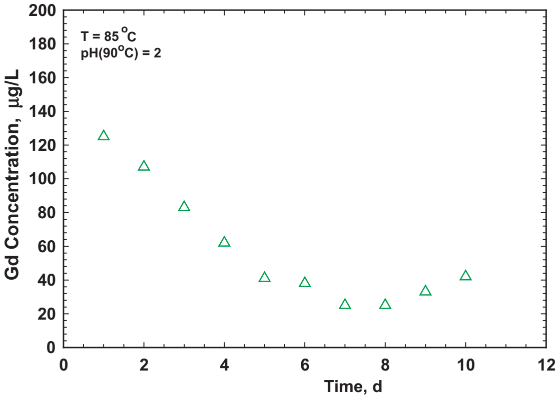

Fig. 28. Results for Gd release from a P1-238 specimen in a SPFT test at a pH of 2 and 85 °C.

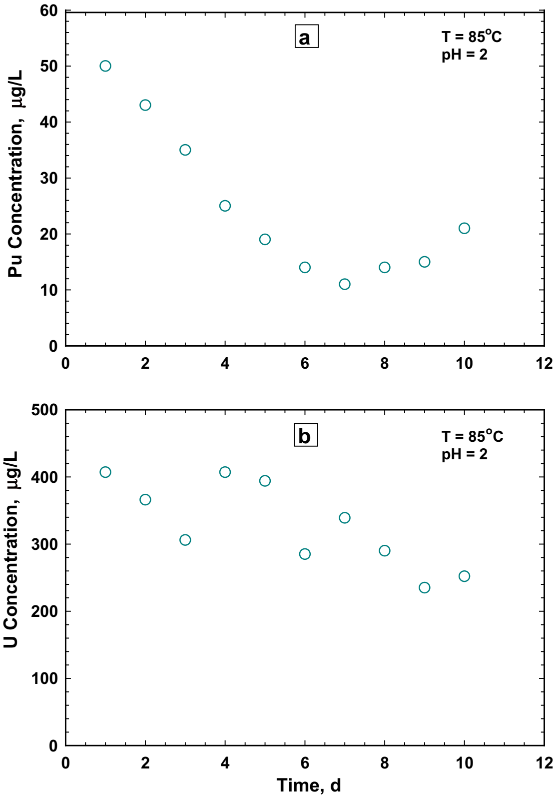

Fig. 29. Results for (a) ^{238}Pu and (b) U Releases from a PI-238 Specimen in a SPFT Test at a pH of 2 and 85 °C.

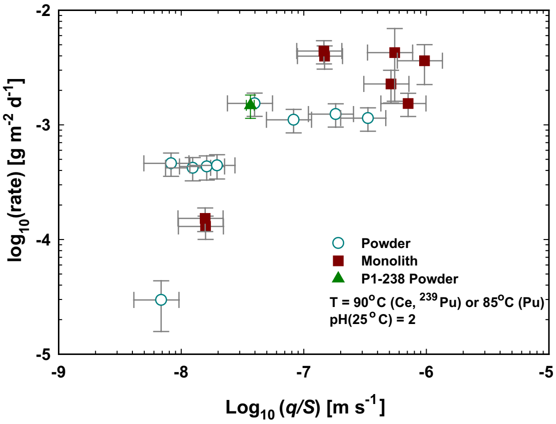

Fig. 30. Results from SPFT tests non-radioactive and non-radioactive pyrochlore-based specimens with compositions similar to the P1 specimens showing the variation of the dissolution rate with increasing q/S.

geometric surface area in our calculations. Visually, the agreement looks worse than it is because the data are plotted on a log–log graph.

3.5.2. PB1 specimens

The release of Gd from the resintered and the fully radiation-damaged (original) PB1-238 specimens is almost identical (Fig. 31). Dissolution rates calculated from steady-state Gd concentrations overlap for the two specimens and are $3.9(10) \times 10^{-4}$ g/(m^2 d) for the radiation-damaged and resintered specimens. Thus, based on the Gd concentrations, there is no difference between the dissolution of undamaged (resintered) and fully damaged (original) specimens. As in the case of the P1-238 specimen, the release of Pu and U from the PB1-238 specimens do not reach steady state. Thus, we can only estimate the steady-state dissolution rate based on the Pu concentrations, while a good value is obtained from the Gd concentrations. Estimated release rates based on ^{238}Pu are $2.4(6) \times 10^{-4}$ and $3.7(8) \times 10^{-4}$ g/(m^2 d) for the radiation-damaged and resintered specimens, respectively, and in reasonable agreement with the value obtained from the Gd concentrations. The release of U to solution follows a pattern similar to that of ^{238}Pu. So, a reasonable steady-state dissolution rate based on the U concentrations can be estimated at $6.7(15) \times 10^{-4}$ g/(m^2 d). For the fully radiation-damaged (original) PB1-238 specimen, the concentration of U continue to decrease after day 6, so we can only estimate the dissolution rate based on U at $8.3(2) \times 10^{-4}$ g/(m^2 d). These dissolution rates are slightly higher than the dissolution rate based on the Gd concentrations. Since the Gd concentration reached steady state and the Pu and U concentrations appear to be decreasing with time, the release of Gd to solution appears to be the most reliable index of dissolution, and the resintered and radiation-damaged PB1-238 specimens dissolve at the same rate. Even though the Pu and U concentrations did not reach steady state, the behavior of both elements for undamaged and fully damaged specimens is the same.

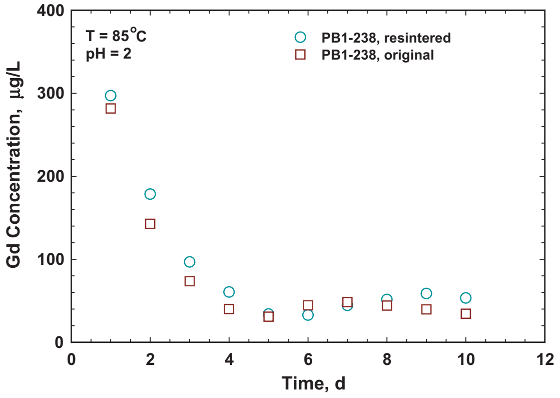

Fig. 31. Results for Gd release from a PB1-238 specimen in a SPFT test at a pH of 2 and 85 °C.

Fig. 32 shows the results for the flow rate dependence, expressed as q/S, of the dissolution rate for radioactive (PB1-238 and PB1-239) and non-radioactive specimens [64]. The rates were computed from the Gd release. The figure shows that, at values of $\log_{10}(q/S)$ [m s^{-1}] < -8, dissolution rates of the PB1 specimens decrease in a manner consistent with a reaction affinity mechanism. At $\log_{10}(q/S)$ values of > -8 the dissolution rate becomes independent of q/S, signifying that release of Gd is at the forward rate of reaction. Note that the two PB1-238 specimens plot on this diagram close to the forward rate of reaction. As with the comparison

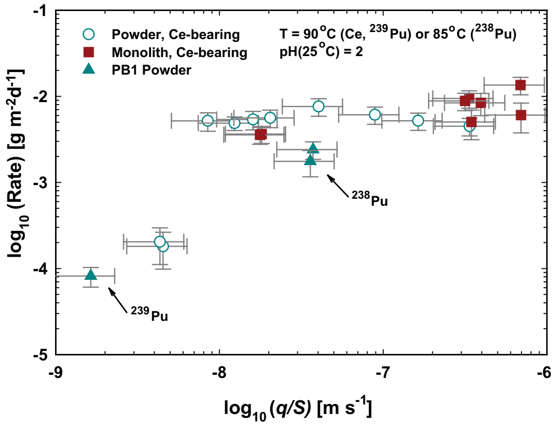

Fig. 32. Results from SPFT tests on radioactive and non-radioactive pyrochlore-based specimens with compositions. Similar to the PB1 specimens showing the variation of the dissolution rate with increasing q/S.

Table 5
Summary of changes to the physical properties of the specimens studied

Physical/chemical property	Storage temperature, °C	Phase	P1-238	PB1-238
'True' density, % decrease	20		6.8, 6.4(c)	11, 11.4
	125		6.4	9.9
	250		5.6	7.4
Volumetric swelling, %	20		7.2, 7.9	4.6, 3.3
Saturation dose, α/g	20		7.3×10^{18}, 3.5×10^{18}, 8.9×10^{18}	2.3×10^{18}
	125		6.7×10^{18}	
	250		6.8×10^{18}	
Unit cell volume, % increase	20	Pyrochlore	3.6	4.6
		Zirconolite		1.1
	250	Pyrochlore	3.0	1.6
		Zirconolite	1.1	1.8
Dissolution Rate, g/(m^2 d)	20		1.3×10^{-3}	7.2×10^{-4}

between the monolithic and the powdered specimens, some of this difference may be attributable to the differences in porosity and effective surface areas. As with the PI specimens, the difference between the monolithic specimens and the powdered specimens is about a factor of 3. Visually, however, the agreement looks better because this is a log–log graph, and the range of the data is between 6×10^{-3} g/(m^2 d) and 9×10^{-3} g/(m^2 d) for the powdered and monolithic specimens, respectively.

To summarize this section, the release of Pu is very slow, even at pH 2 and 85–90 °C. At higher pH values, concentrations of Pu are below the lower limit of quantification, which likely indicates that Pu is solubility limited. Uranium release at pH 2 is also very slow with rates identical to or slightly higher than those based on the Pu concentrations. At higher pH values, the release rate based on U is lower and may also indicate solubility control. The fact that the fully radiation-damaged (original) and resintered ^{238}Pu-bearing specimens yield overlapping dissolution rates means there is no change in dissolution rate from radiation-induced damage. The fact that the dissolution behavior of the fully damaged and resintered Pu-bearing specimens and the non-radioactive specimens is consistent with increasing *q*/*S* means that the forward rate of 1.3×10^{-3} and 7.2×10^{-3} g/(m^2 d) can be obtained from Figs. 30 and 32 for P1 and PB1 specimens, respectively.

4. Summary and conclusions

We studied the effects of radiation-induced damage in two groups of materials each containing several specimens in which damage from the decay of ^{238}Pu accumulated for approximately 1100 days. In the first group, P1 the specimens consisted of two phases, a pyrochlore with the apparent chemical formula $Ca_{1.13}Gd_{0.22}Hf_{0.12}Pu_{0.24}$-$U_{0.40}(Ti_{1.90}Hf_{0.10})O_7$ and Hf-rutile [$(Hf_{0.1}Ti_{0.9})O_2$], containing 20% of the total TiO_2. These phase compositions were estimated from the target composition. In the second group, PB1, the specimens contained four phases, pyrochlore, zirconolite, brannerite, and Hf-rutile. Chemical formulas could not be estimated for the phases in these specimens because suitable analytical instrumentation was unavailable for these highly radioactive specimens. Some of the initial P1 specimens were sintered for an additional 100 h to coarsen the microstructure. This was done to determine if the coarser microstructure material was more susceptible to microcracking; no effect was observed. After approximately 2 years, some of the original specimens from both groups that had become amorphous from radiation-induced damage accumulation were resintered to remove the ingrown radiation-induced damage so that we could determine the changes that occur at low damage accumulation. A summary of results is shown in Table 5.

Photomicrographs of the P1 specimen that was originally stored at 20 °C and was again stored at 20 °C after resintering showed a uniformly dense material consisting of a pyrochlore and a rutile phase. Minor phases were also evident, but they could not be identified, either from the SEM or XRD results. The porosity was limited; no evidence for open porosity changing to closed porosity was discernable in the SEM photomicrographs. However, there was evidence for accumulation of a high or absence of low atomic number component(s) at the grain boundaries. Also noted was the tendency for rutile to exist at the triple points of the grains. Even at magnifications of 10000×, there was no evidence for cracking in the material from radiation-induced swelling. There was also evidence for compositional variability across pyrochlore grains. Although this variation could not be quantified with SEM/EDS, it would be consistent with the observation that zirconolite was stabilized after prolonged heating at 250 °C and radiation-induced damage.

Specimens that were resintered after being stored at ambient and 125 °C each showed different phase assemblages. The XRD patterns from the specimens that had been stored at 20 °C for about 2.5 years and then were resintered showed the presence of only pyrochlore and rutile (TiO_2). The expansion of the a_0 unit cell dimension was determined to be 1.2% over approximately 400 days (2.4×10^{18} α/g). The specimens that had been stored at 125°C before being resintered showed evidence of four phases, pyrochlore, rutile, and two zirconolites, at least one of which had preferred orientation, probably from the defects on the surface of the specimen. The ^{238}Pu appeared to be distributed amongst these phases differently as evidenced from the change in diffraction-peak intensity and broadening with increasing time. We concluded that one zirconolite had more ^{238}Pu than the other. This is in agreement with the SEM results, although we were unable to obtain a quantitative measure of the compositional variation. In the original specimens stored at 250 °C, there was some indication of an in-growth of zirconolite, but not for the specimens stored at 125 °C [51]. Although undetected at 125 °C, the processes were taking place such that they became manifest upon resintering. Pyrochlore and zirconolite phases are prone to lamellae formation [58], and it is possible that lamellae have formed in this material. Apparently, sintering this specimen at 1350 °C for 2 h was insufficient to restore the original pyrochlore phase, and the system was kinetically at a local minimum in the free energy because of the local arrangement of atoms from the radiation-induced damage. This may simply be the result of slower quenching that occurs at higher temperatures in the displacement cascade, or it could represent a phase instability at 125 °C. For example, Helean et al. [36] and Putnam et al. [60] showed that Ce-pyrochlore is metastable with respect to $CaTiO_3$, CeO_2, and TiO_2. Therefore, we conclude that the radiation-induced damage and storage at 125 and 250 °C stabilized perhaps kinetically, a mixture of pyrochlore and zirconolite. These phases became amorphous shortly after the zirconolite formed from the pyrochlore.

After we ended the experiments with the specimens that had been stored at 125 °C, were sintered at 1390 °C for 8 h. The resulting XRD pattern consisted of diffraction from pyrochlore, rutile, and a single zirconolite with preferred orientation. The same result was obtained from the same specimen after it was sintered for an additional 24 h at 1350 °C. These results suggest that, while there may be kinetic barriers to the reformation of pyrochlore from the new phase assemblage, it is also likely that chemical changes have occurred (e.g., oxidation state changes) so that zirconolite is one of the thermodynamically stable phases in these solids.

Results from other studies suggest that Hf might have substituted for Ti in the pyrochlore phase in our specimens. Some Hf substitution on the Ti site was needed to minimize the residuals in the Rietveld fit to the observed XRD patterns. To charge balance the chemical formula, some Hf was needed on the Ti site. Since Hf is included in the formulation as a neutron absorber to control criticality in these materials, and the chemistry of Hf and Zr are very similar. Some Zr-bearing pyrochlore compounds have been shown to resist very high doses without becoming amorphous [65].

We also examined a set of specimens, PB1, in which the dominant phase was pyrochlore with zirconolite, brannerite, and Hf-rutile as other phases, This ceramic is based on the formulation that was to be the target composition for production at the Plutonium Immobilization Plant. The specimen diameters swelled by 1.5%, implying that the bulk density decreased by 4.7%, and the changes appeared to be independent of storage temperature within the experimental uncertainty. The 'true' densities decreased by more than the bulk densities at all temperatures, suggesting that some of the open porosity became closed porosity, the 'true' densities after more than 1300 days ($\sim 8 \times 10^{18}$ α/g or ~980 years when the dose comes from ^{239}Pu in the repository) of accumulated damage were 11%, 9.9%, and 7.4% for the specimens stored at 20, 125, and 250 °C, respectively. Although there is no significant dependence of the macroscopic swelling on temperature, there is a dependence of the 'true' density and the unit cell dimensions on temperature. These observed differences further suggest that open porosity is becoming closed as individual particles swell.

Results from the XRD analyses, show that the PB1 ceramic becomes amorphous by 3.7×10^{18} α/g or about 650 days for these materials. Results from the resintered specimens gave us a better understanding of how the individual phases change with radiation-induced damage. The pyrochlore phase swells by 4.6% at 20 °C over 675 days (~500 years from ^{239}Pu) that was obtained from a least-squares fit of Eq. (2) to the data. At 250 °C, the cell-volume expansion is the same, but it takes 1.8 times longer to achieve that expansion. This is consistent with a decrease in the relative damage volume per alpha event that one expects from thermally activated recovery processes. The brannerite phase is the most sensitive to the effects of radiation damage. This is consistent with the metastability of the brannerite phase [61] and the relative thermodynamic stability of the pyrochlore and zirconolite phases [36]. Since the rutile phase does not contain any Pu [66], the small changes in the lattice parameters were likely caused by the radiation from the surrounding phases containing Pu. The zirconolite phase in the PB1 specimens behaved differently with accumulated damage than zirconolites in other materials in that the major effect of radiation-induced damage was to a_0, b_0, and β and no significant change in c_0. Examination of a sample of this material in the SEM did not provide any information that could be used to explain this difference.

Scanning electron microscope images suggest that zirconolite in the pyrochlore ceramics is embedded (as lamella or veins within the pyrochlore. This might indicate that the zirconolite crystallizes with a preferred orientation. This may be the reason why only specific axes were affected by the radiation effects. It is also clear from the SEM images that brannerite solidifies last during processing and has an ill-defined shape (anhedral). If this phase is poorly crystallized or had the shortest time to form, this coupled with the less favorable thermodynamic properties probably make it less resistant to radiation effects than the other phases. The SEM images also indicate that undissolved actinide inclusions are usually present near the brannerite, possibly increasing the radiation field around it and perhaps suggesting that more Pu was soluble at sintering temperatures.

We used the SPFT technique to determine the dissolution behavior of these ceramics. Specimens made from non-radioactive chemicals [64] or with Pu and U (the work reported here) have been tested with solutions over a pH range of 2–12 at 85–90 °C. For the ^{238}Pu-bearing specimens, a SPFT test apparatus constructed from titanium was used to reduce or eliminate materials and radiolysis effects on the test result. The results show that there is no difference within experimental uncertainty in the dissolution rates between non-radioactive, ^{239}Pu-, and ^{238}Pu-bearing ceramics when the q/S value is high. Pyrochlore (P1 specimens) and a ceramic containing four phases (PB1 specimens) initially have forward dissolution rates of 1.3×10^{-3} and 7.2×10^{-4} g/(m^2 d), respectively. Hence, the high dissolution rates we reported earlier [53,67] were a result of radiolysis effects on the leachant that caused enhanced dissolution. These results indicate that, for the titanate materials tested, there is no change in the dissolution rate of the immobilized Pu form from radiation-induced damage.

From a physical point of view, both ceramics appear to be a viable for the immobilization of Pu. Although pyrochlore would become X-ray amorphous in a relatively short time, after approximately 300 years in the repository, the material would maintain its physical integrity with no observable microcracking over the time during which physical changes are predicted to saturate (950 years). The accumulated alpha dose (about 7.5×10^{18} α/g for the P1 specimens) to the specimens studied in the work presented here is equivalent to approximately 970 years of storage of ^{239}Pu-bearing pyrochlore ceramic waste form.

Irrespective of composition, P1 or PB1, there was no evidence of microcracking. Physically, the specimens remained intact. No evidence for microcracking was evident during the SEM examinations of this material. Thus, although pyrochlore is susceptible to radiation-induced damage, the material remains viable as a material for immobilizing surplus weapons-grade Pu.

Acknowledgements

The authors wish to acknowledge the contributions to this work of persons whose assistance was very much appreciated. Many helpful discussions were held with David McCready (PNNL) on the interpretation of the X-ray results and the use of the Rietveld program and with Bill Weber (PNNL) on the effects of radiation damage. Work with these quantities of ^{238}Pu would not have been possible without the assistance of the radiation protection and safety personnel at PNNL. While working within the guidelines for protection and safety, they made helpful suggestions as to how certain activities could take place. Todd Schaef played an important role in facilitating the use of an X-ray diffractometer with these highly radioactive materials. The financial assistance from the Department of Energy is gratefully acknowledged, in the long-term programmatic support from Mr William Danker[3] and Andre Cygelman is particularly appreciated. Pacific Northwest National Laboratory is operated for the US Department of Energy by Battell under Contract DE-AC05-76RL01830.

References

[1] USA, Agreement between the Government of the United States of America and the Government of the Russian Federation concerning the management and disposition of plutonium designated as no longer required for defense purposes and related cooperation, United States Department of State, 2000.

[2] US Department of Energy (DOE). Report to Congress: Disposition of surplus defense plutonium at Savannah River site. Department of Energy, Washington, DC, 2002.

[3] US Department of Energy (DOE). Amended record of decision for the surplus plutonium disposition program. Office of the Federal Register, Washington, DC, 2002.

[4] M.W Stokes, E.L. Hovis, E.L. Hamilton, J.B. Fiscus, Plutonium Immobilization Canister Loading,

---

[3] Currently at the International Atomic Energy Agency, Vienna, Austria.

WSRC-TR-00441, Westinghouse Savannah River Co., Aiken, SC, 1999.

[5] B.R. Myers, G.A. Armantrout, C.M. Jantzen, A. Jostsons, J.M. McKibben, H.R. Shaw, D.M. Strachan, J.D. Vienna, Technical evaluation panel summary report: ceramic and glass immobilization options, UCRL-ID-129315, Livermore National Laboratory, Livermore, CA, 1998.

[6] S.G. Cochran, W.H. Dunlop, T.A. Edmunds, T.H. Gould, L.M. MacLean, Fissile material disposition program: final immobilization form assessment and recommendation, Lawrence Livermore National Laboratory Livermore, CA, 1997.

[7] B.B. Ebbinghaus, C. Cicero-Herman, L. Gray, H.F. Shaw, Plutonium immobilization project: baseline formulation, UCRL-ID-133089, Lawrence Livermore National Laboratory, Livermore, CA, 1999.

[8] TRW, Degraded mode criticality analysis of immobilized plutonium waste forms in a geologic repository, A00000000-01717-5705-00014 Rev 01. TRW Environmental Safety Systems, Inc., Las Vegas, NV, 1997.

[9] F.W. Clinard, D.L. Rohr, in: J.G. Moore (Ed.), Scientific Basis for Nuclear Waste Management, Plenum, NY, 1981, p. 405.

[10] F.W. Clinard, C.C. Land, D.E. Peterson, D.L. Rohr, R.B. Roof, Mater. Res. Soc. Symp. Proc. 6 (1982) 405.

[11] W.J. Weber, R.C. Ewing, C.R.A. Catlow, T. Diaz de la Rubia, L.W. Hobbs, C. Kinoshita, H. Matze, A.T. Motta, M. Nastasi, E.K.H. Salje, E.R. Vance, S.J. Zinkle, J. Mater. Res. 13 (1998) 1434.

[12] R.L. Fleischer, Geo. Cosmohim. Acta 67 (2003) 4769.

[13] J.W. Wald, W.J. Weber, Adv. Ceram. Nucl. Waste Manage. 8 (1984) 71.

[14] W.J. Weber, J.W. Wald, H. Matzke, Mater. Lett. 3 (1985) 173.

[15] W.J. Weber, J.W. Wald, H. Matzke, J. Nucl. Mater. 138 (1986) 196.

[16] W.J. Weber, H. Matzke, Radiat. Eff. 98 (1986) 93.

[17] S.X. Wang, L.M. Wang, R.C. Ewing, J. Non-Cryst. Sol. 274 (2000) 238.

[18] B.E. Burakov, E.B. Anderson, M. Yagovkina, M. Zamoryanskaya, E. Nikolaeva, J. Nucl. Sci. Technol. (Suppl. 3) (2002) 733.

[19] B.E. Burakov, E.B Anderson, M. Yagovkina, M. Zamoryanskaya, E. Nikolaeva, Behavior of ^{238}Pu-doped ceramics based on cubic zirconia and pyrochlore under radiation damage, in: Actinide 2001 International Conference, Atomic Energy Society of Japan, Japan, 2002, p. 733.

[20] A.N. Lukinykh, S.V. Tomilin, A.A. Lizin, A.A. Yelesin, A.G. Yakovenko, A.V. Bychkov, Investigation of chemical resistance and structural restoration of damaged titanate ceramics designed for actinides disposal. SSC RF RIAR, Dimitrograd, Russia, 2002.

[21] Y.F. Volkov, S.V. Tomilin, A.N. Lukinykh, A.A. Lizin, A.A. Elesin, A.G. Yakovenko, V.I. Spiryakov, A.V. Bychkov, L.J. Jardine, Radiochemistry 46 (2004) 351.

[22] Y.F. Volkov, S.V. Tomilin, A.N. Lukinykh, A.A. Lizin, A.A. Elesin, A.G. Yakovenko, V.I. Spiryakov, V.I. Konovalov, V.M. Chistyakov, A.V. Bychkov, L.J. Jardine, Radiochemistry 46 (2004) 358.

[23] R.C. Ewing, W.J. Weber, J. Lian, J. Appl. Phys. 95 (2004) 5949.

[24] J.W. Wald, P. Offerman, in: W. Lutze (Ed.), Scientific Basis for Nuclear Waste Management V, North Holland, New York, 1982, p. 369.

[25] J.W. Wald, P. Offerman, Mater. Res. Soc. Symp. Proc. 11 (1982) 369.

[26] S.X. Wang, L.M. Wang, R.C. Ewing, G.S. Was, G.R. Lumpkin, Nucl. Instrum. and Meth. Phys. Res. B 148 (1999) 704.

[27] J. Chen, J. Lian, L.M. Wang, R.C. Ewing, L.A. Boatner, Appl. Phys. Lett. 79 (2001) 1989.

[28] S.X. Wang, L.M. Wang, R.C. Ewing, K.V. Govindan Kutty, Nucl. Instrum. and Meth. Phys. Res. B 169 (2000) 135.

[29] A. Meldrum, C.W. White, V. Keppens, L.A. Boatner, R.C. Ewing, Phys. Rev. B. 63 (2001) 1.

[30] S.X. Wai g, L.M. Wang, R.C. Ewing, K.V. Govindan Kutty, Mater. Res. Soc. Symp. Proc. 540 (1999).

[31] F.W. Clinard, L.W. Hobbs, C.C. Land, D.E. Peterson, D.L. Rohr, R.B. Roof, J. Nucl. Mater. 105 (1982) 248.

[32] B.D. Begg, W.J. Weber, R. Devanathan, J.P. Icenhower, S. Thevuthasan, B.P. McGrail, Ceram. Trans. 107 (2000) 553.

[33] G.R. Lumpkin, R. Gieré, T.E. Payne, P.J. McGlinn, K.P. Hart, Mater. Res. Soc. Symp. Proc. 663 (2001) 989.

[34] Y. Eyal, G.R. Lumpkin, R.C. Ewing, Mater. Res. Soc. Symp. Proc. 84 (1987) 635.

[35] G.R. Lumpkin, J. Nucl. Mater. 289 (2001) 136.

[36] K.B. Helean, A. Navrotsky, E.R. Vance, M.L. Carter, B. Ebbinghaus, O.H. Krikorian, J. Lian, L.M. Wang, J.G. Catalano, J. Nucl. Mater. 303 (2002) 226.

[37] R.L. Putnam, A. Navrotsky, B.F. Woodfield, J.L. Shapiro, R. Stevens, J. Boerio-Goates, Mater. Res. Soc. Symp. Proc. 556 (1999) 11.

[38] D.M. Strachan, R.D. Scheele, W.C. Buchmiller, J.D. Vienna, R.L. Sell, R.J. Elovich, Preparation and characterization of ^{238}Pu-ceramics for radiation damage experiments, PNNL-13251, Pacific Northwest National Laboratory, Richland, WA, 2000.

[39] P.K. Saripalli, B.P. McGrail, D.C. Girvin, Appl. Geochem. 17 (2002) 649.

[40] M.W.A. Stewart, E.R. Vance, A. Jostsons, K. Finnie, R.A. Day, B.B. Ebbinghaus, Mater. Res. Soc. Symp. Proc. 713 (2002) 381.

[41] L. Minervinni, R.W. Grimes, K.E. Sickafus, J. Am. Ceram. Soc. 83 (2000) 1873.

[42] B.D. Begg, N.J. Hess, D.E. McCready, S. Thevuthasan, W.J. Weber, J. Nucl. Mater. 289 (2001) 188.

[43] N.J. Hess, B.D. Begg, S.D. Conradson, D.E. McCready, P.L. Gassman, W.J. Weber, J. Phys. Chem. B 106 (2002) 4663.

[44] R. Gieré, C. Hatcher, E. Reusser, E.C. Buck, Mater. Res. Soc. Symp. Proc. 713 (2002) 303.

[45] J.A. Fortner, A.J. Kropf, R.J. Finch, A.J. Bakel, M.C. Hash, D.B. Chamberlain, J. Nucl. Mater. 304 (2002) 56.

[46] S.D. Conradson, Appl. Spectrosc. 52 (1998) 252a.

[47] B.E. Burakov, E.B. Anderson, Immobilization of excess weapons plutonium in Russia: a review of LLNL contract work, UCRL-ID-143846, Lawrence Livermore National Laboratory Livermore, CA, 2001.

[48] Y.F. Volkov, A.N. Lukinykh, S.V. Tomilin, A.V. Bychkov, Immobilization of excess weapons plutonium in

Russia, UCRL-ID-143846, Lawrence Livermore National Laboratory Livermore, CA, 2001.

[49] D.M. Strachan, H.T. Schaef, M.J. Schweiger, K.L. Simmons, L.J. Woodcock, M.K. Krouse, Powder Diffract. 18 (2003) 23.

[50] D.M. Strachan, W.C. Buchmiller, W.R. Park, J.T. Munley, Instrum. Sci. Technol. 32 (2004) 1.

[51] D.M. Strachan, R.D. Scheele, J.P. Icenhower, B.C. Buck, A.E. Kozelisky, R.L. Sell, RJ. Elovich, W.C. Bichmiller, Radiation damage effects in candidate ceramics for plutonium immobilization: final report, PNNL-14588, Pacific Northwest National Laboratory, Richland, WA, 2004.

[52] D.M. Strachan, R.D. Scheele, A.E. Kozelisky, R.L. Sell, H.T. Schaef, M.J. O'Hara, C.F. Brown, W.C. Bichmiller, Radiation damage in titanate ceramics used for plutonium immobilization, PNNL-SA-35541, Pacific Northwest National Laboratory, Richland, WA, 2001.

[53] J.P. Icenhower, D.M. Strachan, M.J. Lindberg, E.A. Rodriguez, J.L. Steele, Dissolution kinetics of titanate-based ceramic waste forms: results from single-pass flow tests on radiation damage specimens, PNNL-14252, Pacific Northwest National, Laboratory, Richland, WA, 2003.

[54] D.M. Strachan, R.D. Scheele, A.E. Kozelisky, R.L. Sell, H.T. Schaef, M.J. O'Hara, C.F. Brown, W.C. Buchmiller, Mater. Res. Soc. Symp. Proc. 713 (2002) 461.

[55] D.M. Strachan, R.D. Scheele, A.E. Kozelisky, R.L. Sell, Effects of self irradiation from ^{238}Pu on candidate ceramics for plutonium immobilization, PNNL-14232, Pacific Northwest National Laboratory, Richland, WA, 2003.

[56] F.W. Clinard, Am. Ceram. Soc. Bull. 65 (1986) 1181.

[57] H.F. Shaw, Determination of the open and closed porosity in an immobilized Pu ceramic wasteform, UCRL-ID-132605, Lawrence Livermore National Laboratory, Livermore, CA, 1998.

[58] E.C. Buck, D.B. Chamberlain, R. Gieré, Mater. Res. Soc. Symp. Proc. 556 (1999) 19.

[59] C.J. Howard, T.M. Sabine, J. Phys. C: Solid State Phys. 7 (1974) 3453.

[60] R.L. Putnam, K.B. Helean, A. Navrotsky, E.C. Buck, B.B. Ebbinghaus,H.F. Shaw, E.R. Vance, M.A. Williamson, Plutonium immobilization project: limits of thermodynamic stability of pyrochlore waste forms for surplus weapons plutoniutn, UCRL-JC-13509, Lawrence Livermore National Laboratory, Livermore, CA, 1999.

[61] K.B. Helean, A. Navrotsky, G.R. Lumpkin, M. Colella, J. Lian, R.C. Ewing, B. Ebbinghaus, J.G. Catalano, J. Nucl. Mater. 320 (2003) 231.

[62] E.R. Vance, M.L. Carter, G.R. Lumpkin, R.A. Day, B.D. Begg, Solid solubilities of Pu, U, Gd, and Hf in candidate ceramic nuclear wasteforms. Australian Nuclear Science and Technology Organisation, Menai, NSW, Australia, 2001.

[63] B. Ebbinghaus, R.A. Van Konynenburg, E.R. Vance, A. Jostons, R.G. Anthony, C.V. Philip, D.J. Wronkievicz, in: Plutonium Stabilization and Immobilization Workshop, US Department of Energy, 1995.

[64] J P. Icenhower, D.M. Strachan, B.P. McGrail, R.D. Scheele, E.A. Rodriguez, J.L. Steele, M.J. Lindberg, American Mineralogist, accepted for publication.

[65] S.X. Wang, B.D. Begg, L.M. Wang, R.C. Ewing, W.J. Weber, K.V. Govindan Kutty, J. Mater. Res. 14 (1999) 4470.

[66] B. Ebbinghaus, O.H. Krikorian, Ternary phase diagrams that relate to the plutonium immobilization ceramic, UCRL-ID-143170, Lawrence Livermore National Laboratory, Livermore, CA, 2001.

[67] D.M. Strachan, R.D. Scheele, J.P. Icenhower, A.E. Kozelisky, R.L. Sell, V.L. Legore, H.T. Schaef, M.J. O'Hara, C.F. Brown, W.C. Buchmiller, The status of radiation damage experiments, PNNL-13721, Pacific Northwest National Laboratory, Richland, WA, 2001.